How Cosmological Flatness Affects Neutrino Properties

Aaron Smith

A senior thesis submitted to the faculty of
Brigham Young University
in partial fulfillment of the requirements for the degree of

Bachelor of Science

Eric Hirschmann, Advisor

Department of Physics and Astronomy

Brigham Young University

August 2012

ABSTRACT

How Cosmological Flatness Affects Neutrino Properties

Aaron Smith
Department of Physics and Astronomy
Bachelor of Science

Cosmological data provide new constraints on the number of neutrino species and neutrino masses. However these constraints depend on assumptions related to the underlying cosmology. Since a correlation is expected between the number of effective neutrinos N_{eff}, the total neutrino mass $\sum m_\nu$, and the curvature of the universe Ω_k, it is useful to investigate the current constraints in the framework of a nonflat universe. We provide an introduction to modern cosmology, placing an emphasis on topics relevant to constraining neutrino parameters with the latest cosmic microwave background (CMB) anisotropy data. The theoretical framework is designed to condense a wide variety of resources and make them available for students with similar research interests. We consider how cosmological flatness affects neutrino properties by providing theoretical arguments for correlation and performing statistical analyses on cosmological models involving neutrinos. We place new constraints on N_{eff} and Ω_k, with $N_{eff} = 4.03 \pm 0.45$ and $10^3\,\Omega_k = -4.46 \pm 5.24$. Thus, even with a nonflat universe, $N_{eff} = 3$ is still disfavored with 95% confidence. We then investigate the correlation between neutrino mass $\sum m_\nu$ and curvature Ω_k that shifts the 95% upper limit of $\sum m_\nu < 0.45$ eV to $\sum m_\nu < 0.95$ eV. Thus, the impact of assuming flatness should be an essential consideration for future neutrino analysis in experimental cosmology.

Keywords: cosmology, cosmic microwave background, effective neutrino number, neutrino mass, curvature

ACKNOWLEDGMENTS

I would like to thank Eric Hirschmann and David Neilsen for teaching me general relativity and its applications in astrophysics. I am grateful for my association with Jeff Humpherys, Shane Reese, and the fellow cohorts from the Interdisciplinary Mentoring Program in Analysis, Computation, and Theory (IMPACT) (See http://impact.byu.edu/). I also thank Jean-François Van Huele and Michael Ware for teaching the advanced writing course for physics at Brigham Young University. Finally, this research was started as a visiting undergraduate summer researcher at the Center for Cosmology at the University of California, Irvine. I thank my coauthors Maria Archidiacono, Asantha Cooray, Francesco De Bernardis, Alessandro Melchiorri, and Joseph Smidt (See http://arxiv.org/abs/1112.3006 or Ref. [1]). This research was supported in part by NSF CAREER AST-0645427 to Asantha Cooray and the Department of Physics and Astronomy at BYU.

Contents

List of Figures

Chapter 1

Introduction

Where do we fit in the grand scheme of things? Non-scientific searches can lead to very different answers, but for many this discovery motivates a systematic approach to understanding the cosmos. In the realm of the observable Universe this is exactly what cosmology is about! In fact, fundamental physical principles allow scientists to "put a face" to the Universe. The precise questions addressed in this work involve the mysterious properties of neutrinos, which are weakly interacting, electrically neutral leptons important for nuclear decay processes. The standard model of particle physics allows for three types of massless neutrinos, however, it is now known that this picture is incomplete because neutrinos do have mass! Furthermore, cosmological data place doubt on the effective number of neutrino species. This chapter provides the necessary context and background required in order to study the properties of neutrinos from a cosmological perspective.

1.1 Evidence for additional neutrino species

Data from the cosmic microwave background (CMB) provide constraints on the composition and structure of the Universe. The most recent data suggests the presence of more than three effective neutrino species N_{eff}. Indeed, a recent paper claims that "the number of neutrinos is greater than

the standard model value with 98.4% confidence" [2]. This statistic, as radical as it may appear, has been substantiated by others undertaking similar analysis with cosmological data (cf. [3, 4]). Throughout the thesis we are comfortable with the notion of additional neutrino species.

Where do these additional neutrinos come from? No one yet knows for sure, but theorists offer several possibilities. We briefly mention some ideas but stress a detachment from excessive speculation on this topic. The more exotic models include arguments for sterile neutrinos or modified dark energy [5–7]. Indeed, an increasing number of cosmologists and particle phenomenologists prescribe to a (3+1) or (3+2) model for neutrinos. This includes three active massive neutrinos and one or two sterile neutrinos [8, 9]. In this work we emphasize that the "effective neutrino number" is just that—effective. In other words, although something is producing the same signature in CMB data as neutrinos, the effect may be due to something entirely different than physical neutrinos. Therefore, the high neutrino number does not necessarily debunk what has been learned from the standard model of particle physics. At this point we postpone further discussion about cosmological neutrino physics until Section 1.4, where the properties are described in full detail.

This thesis explores possibly overlooked parameter degeneracy with the curvature of the Universe. If the parameter space is degenerate, or admits correlation, then statistical analysis is silent as to whether a result is due to the original parameter or the related parameter. In general, the freedom from such degeneracy is decreased with each improved experiment because parameter constraints are tightened. At the same time if additional parameters are considered in a model then the uncertainty of degenerate parameters increases. The qualitative effect is shown in Fig. 1.1 with a distribution, or 'cloud,' of data for the parameters under consideration. In fact, the distribution will change based on the assumptions made by the model. The strength of the correlation is a good indication that there may be deeper physical connections between the parameters. Thus, we attempt to explain degeneracy and hope for an extended parameter space more consistent with the standard model value of three neutrino species. The key concept is that statistical analysis of CMB

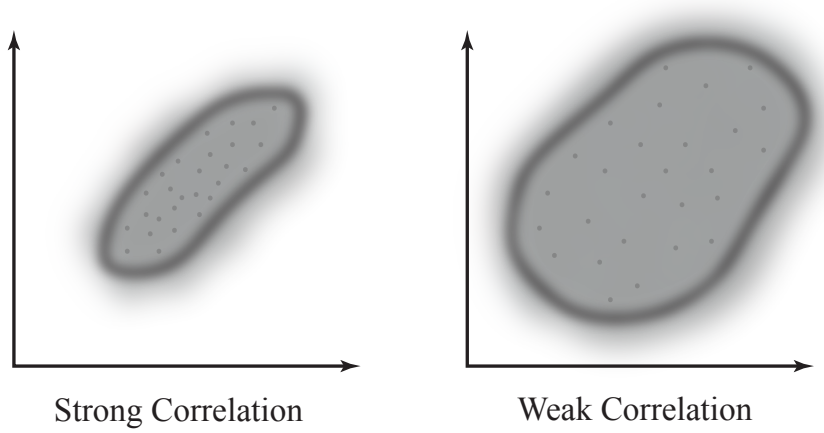

Figure 1.1 Examples of strong (left) and weak (right) correlation. Following Hubble's work in 1929, one might infer a relationship between distance and radial velocity among extra-galactic nebulae. In an analogous manner, the assumptions made by the model may produce slightly different outcomes and infer different contour constraints. The axes are intentionally left blank to focus on the strength of the correlations, however, one might imagine plotting doppler redshift as a function of distance.

data are specific to the prescribed model. Thus, a model may be driven by physical principles but the data may provide surprising results (e.g. cosmic acceleration, additional neutrinos, etc.). With this motivation in mind, evidence for correlation between curvature and neutrino properties is revealed by the theoretical arguments of Chapter 2 and computational results of Chapter 3.

1.2 The cosmic microwave background

Experimental cosmology has benefited from accurate measurements of the cosmic microwave background (CMB) [10, 11]. Data from the CMB is emphasized in this thesis because of the recent cosmological advances gained from it. However, CMB data is coupled with other experiments, such as redshift surveys, to provide improved statistical inference. Current parameter estimation from the CMB focuses on tightening fundamental constraints [11–13] as well as exploring models for extended parameter spaces [14]. The data have determined constraints on several cosmological

parameters to remarkable accuracy, including parameters not included in standard models [15]. Furthermore, the ability to constrain new physics with the CMB continues to improve (Contrast the progress made between [16] and [11] constraints). Future CMB experiments may even be able to settle outstanding questions in cosmology. Some examples are early magnetic B-mode polarization effects from the Big Bang [17] and discrimination of competing neutrino mass models (see Subsection 1.4.2 and Refs. [18, 19]). The physical insight from these measurements may be as important to modern cosmology as the discovery of the dark energy acceleration of the Universe.

The cosmic microwave background is one of the most powerful probes of the early universe. In fact, the CMB is comprised of the first photons able to travel through space without being scattered by the dense but expanding Universe. This "surface of last scattering" formed approximately $380,000$ years after the Big Bang is the oldest radiation that cosmologists can currently detect. Before the CMB, the Universe formed in a state of approximate equilibrium, so the measured radiation is manifest by an omnipresent blackbody spectrum in the microwave range. This is the source of the $3\,\mathrm{K}$ background temperature of space, as measured by the COsmic Background Explorer (COBE) satellite. The COBE blackbody curve shown in Fig. 1.2 is so precise that the error bars are too small to be seen. The result is that "theory and observation agree," or in other words the Universe is extremely isotropic (i.e. it looks the same in every direction). Although the quality of COBE was phenomenal for its time, CMB data has improved dramatically since the COBE result. So much so that the CMB has become the iconic testing ground for the physics of Big Bang cosmology [20, 21].

With the aid of precision experiments the slight deviations from isotropy may be measured and connected to the underlying physics. In fact, the deviations from blackbody equilibrium predict observable anisotropies in different parts of the sky. This should be expected because we know the structure of the Universe forms anisotropic clumps (i.e. stars, galaxies, or clusters of galaxies). These predicted temperature fluctuations are sensitive to cosmological parameters which allows

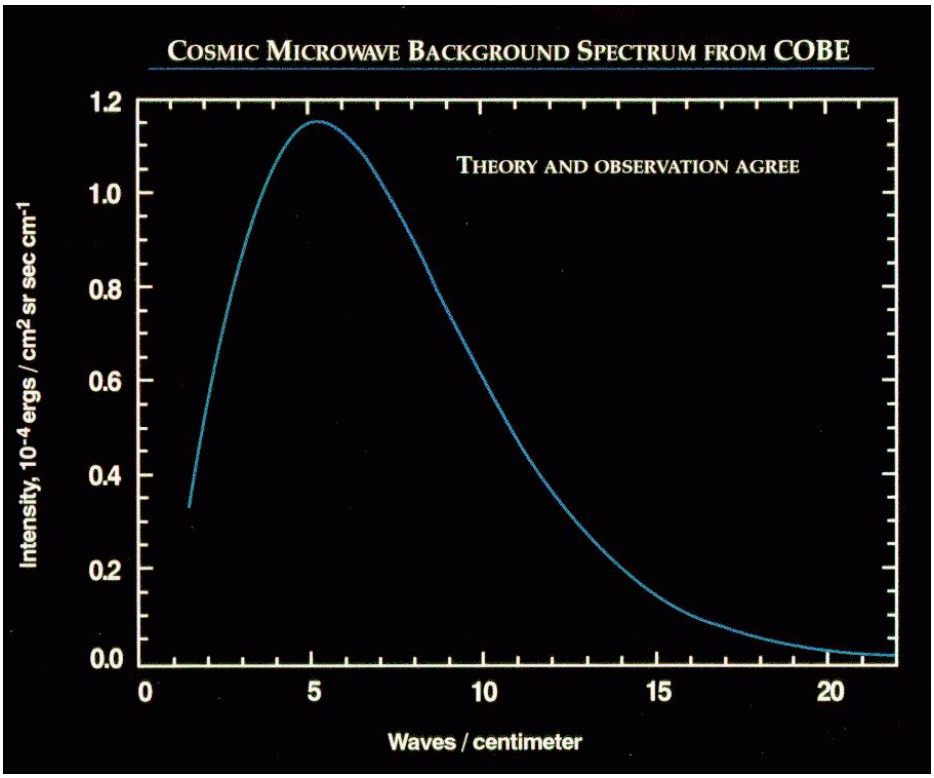

Figure 1.2 The $2.725 \pm 0.002K$ blackbody curve of the CMB as measured by the COBE satellite. John Mather and George Smoot were awarded the 2006 Nobel Prize in Physics for the first detection of the CMB temperature fluctuations. The error bars are too small to be seen in the plot, which explains the phrase "theory and observation agree." The unit along the vertical axis is $\text{erg}\,(\text{cm sr sec})^{-1}$, which is related to SI units by $1\,\text{MJy sr}^{-1} = 2.9979 \times 10^{-7}\,\text{erg}\,(\text{cm sr sec})^{-1}$. Figure from Ref. [22].

statistical constraints to be placed on the model parameters. The information regarding CMB anisotropies is best described by a harmonic decomposition to form the temperature power spectrum. The large scale structure of the universe is a consequence of early cosmological events and the rich physics thereafter (See Section 1.3.1).

Finally, we conclude this section with a summary of the various experiments designed to measure the fluctuations in the CMB. The Wilkinson Microwave Anisotropy Probe (WMAP) has collected seven years of anisotropy data across the entire sky [11]. The scope and experience of WMAP have set the standard for analysis of the temperature power spectrum, however, the resolu-

tion is not high enough to measure very small scale CMB fluctuations. For high multipole modes in the spherical harmonic decomposition there are ground based experiments. In fact, the South Pole Telescope (SPT) [12] and the Atacama Cosmology Telescope (ACT) [13] are complementary to WMAP because they have the resolution for the smallest scales but only cover a small portion of the sky. Thus, WMAP satellite can be used for low mode spectral data ($\ell < 900$) and the ground based experiments SPT or ACT can be used for high modes (up to $\ell \approx 10,000$), a portion of the spectrum referred to as the "damping tail" [23, 24]. SPT and ACT are also at different bandwidths so the combination may provide additional insights. It is hoped that upcoming Planck data will further improve our understanding of cosmological parameters [19, 25], but at this point we proceed with the latest publicly available data. Before we explore the specific methods of constraining cosmological parameters (See Chapter 2) we review some key concepts in modern cosmology.

1.3 Modern cosmology

1.3.1 Cosmic history

In the context of a Big Bang cosmology, the Universe has undergone epochs of both rapid change and slow structural evolution. We now provide a timeline of significant events in cosmic history in order to give context to the importance of CMB data. It is also important to understand the early Universe because the initial conditions help determine the remainder of the structural evolution. Furthermore, the energies attained during the first second of cosmic history are significantly higher than any experiment on earth so cosmology may be the ultimate arena for exploring questions about fundamental physics. In particular it requires an extension of gravity to scales that are small enough for quantum effects to play a significant role. The events of the early Universe happen quickly so hang in there as we start with the first second!

Currently, a theory known as "inflation" proposes a period of rapid expansion as the grand

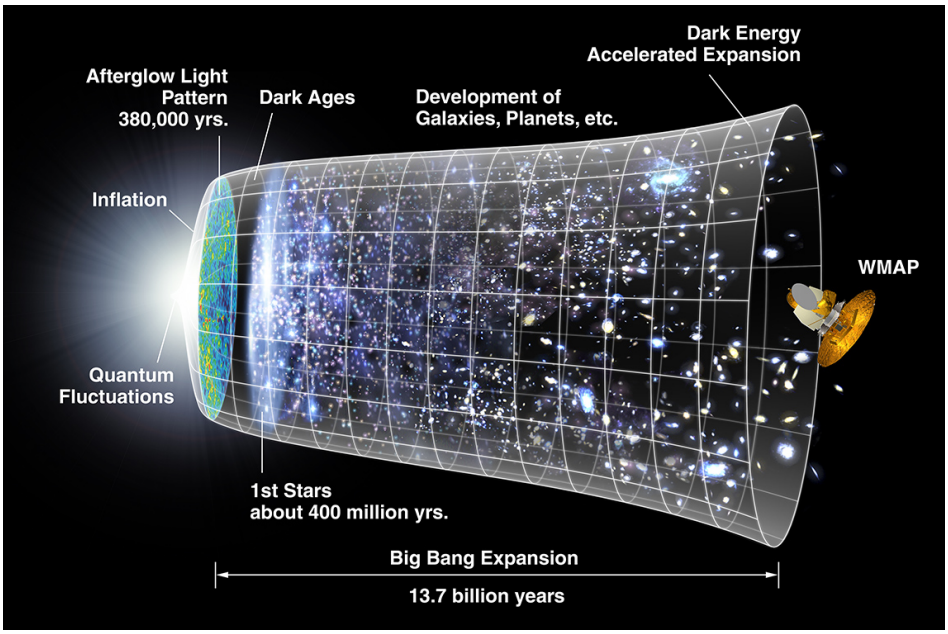

Figure 1.3 A graphical timeline of significant events in cosmic history. Figure from Ref. [26].

advent of the Universe. The expansion from inflation acted to smooth out any unevenness in the primordial spacetime, however, small quantum fluctuations were also blown up to astronomical sizes. This properly explains both the large scale homogeneity of space and the emergence of galaxies from the preexisting overdensities. Now it is somewhat meaningless to talk about times before 10^{-43} s because this corresponds to distances shorter than the Planck length, $\ell_p = \sqrt{\hbar G/c^3}$. In fact, events up to about 10^{-36} s are not well understood because they occur at energies higher than those found in most Grand Unified Theories (GUT). However, around this time inflation kicks in and lasts until at least 10^{-33} s. This is a hot topic of research in cosmology but all inflationary models include a source of negative pressure density to drive expansion. After inflation ends the Universe continues to cool as it expands. Then by around 10^{-10} s (corresponding to an energy of 1 TeV), the "cosmic plasma" has gone through supersymmetry (SUSY) breaking and baryogenesis (*i.e.* the process that produced more baryons than antibaryons). At this point the governing physics is well understood and we may trace out the evolution through the quark-hadron transition (10^{-4} s),

nucleon freeze-out (10^{-2} s), neutrino decoupling (1 s), and Big Bang nucleosynthesis (BBN at 3 minutes). This completes the rapid evolutionary "bang" of the Big Bang.

The next 13.7 billion years is determined by the cooling effects of expansion. The Universe was first dominated by radiation produced from the Big Bang, then was dominated by matter throughout structure formation, and is currently dominated by dark energy. The important event for the CMB is called recombination ($\sim 380,000$ years) because this is when the cosmic plasma is cold enough for electrons to "recombine" with their constituent nuclei. After this point, the Universe enters a period known as the "dark ages" because very little is happening. The situation is one of no stars or galaxies. Instead a tenuous medium of neutral atoms float around with very small departures from homogeneity. Eventually, gravitational attraction localizes any overdensities to regions where inflation ended soonest. This process is called "seeding" because the matter clumps together through weblike structures that will eventually become stars and galaxies. The first photon signals after the dark ages come from the reheating of the Universe as matter collects. Thus the era is aptly named "reionization" because electrons disassociate from their corresponding nuclei. Finally, galaxies as we know them first began to form when the Universe was about half a billion years old. As telescope technology improves over time we may observationally track the statistical properties of the large scale structure to the present time. Our own solar system was formed over five billion years ago. See Fig. 1.3 for a graphical timeline of these significant events in cosmic history. We will revisit particular epochs as needed during further discussion.

1.3.2 Relativistic framework

In general, the physics of the entire Universe is much too complicated to handle exactly so we use models to approach the problem one step at a time. In this sense it is important to realize the mathematics we introduce is used as a tool to understand the underlying physics. Thus, in the framework of relativistic cosmology the fluctuations in the CMB originate as perturbations of

much simpler cosmological solutions in general relativity. We review the most relevant aspects of relativity for cosmological applications and refer the reader to Refs. [20, 27] for more detailed treatments. The *metric* is a geometric tool that relates distances in spacetime, a kind of generalized pythagorean theorem where the time coordinate is included as well. The underlying physics is more important than the relative coordinates, so all equations are written in the invariant language of tensors, or multi-indexed objects. The Einstein summation convention shortens the notation by assuming an implied sum over repeated indices. With this in mind, the Friedmann-Robertson-Walker (FRW) metric for a flat, homogeneous, and isotropic universe in cartesian coordinates (t,x,y,z) is

$$g_{\mu\nu} = \begin{pmatrix} -1 & 0 & 0 & 0 \\ 0 & a^2(t) & 0 & 0 \\ 0 & 0 & a^2(t) & 0 \\ 0 & 0 & 0 & a^2(t) \end{pmatrix}, \tag{1.1}$$

which induces the following line element for measuring infinitesimal distances:

$$ds^2 = g_{\mu\nu} dx^\mu dx^\nu = -dt^2 + a^2(t)\left(dx^2 + dy^2 + dz^2\right). \tag{1.2}$$

Note that in spacetime, the components $dx^\mu = (dt, dx, dy, dz)$ are treated on equal footing except for a relative minus sign in front of the squared time component. However, this allows for the propagation of light along null vectors (i.e. $ds^2 = 0$).

In fact, the Lorentzian form of the metric, *i.e.* the $(-+++)$ signature asymmetry of time with space, explains the presence of a gravitational force in curved spacetime. The geometry is essential so we define vector fields at each point and parallel transport vectors from nearby points to establish a generalized notion of the derivative. For the covariant derivative ∇ this is done by

defining the Christoffel symbols Γ as a way to connect different points in spacetime:

$$\partial \to \nabla \quad \text{where} \quad \nabla_\mu T^\alpha_\beta = \partial_\mu T^\alpha_\beta + \Gamma^\alpha_{\sigma\mu} T^\sigma_\beta - \Gamma^\sigma_{\mu\beta} T^\alpha_\sigma \tag{1.3}$$

$$\text{and} \qquad \Gamma^\mu_{\alpha\beta} = \frac{1}{2} g^{\mu\nu} \left[g_{\alpha\nu,\beta} + g_{\beta\nu,\alpha} - g_{\alpha\beta,\nu} \right] . \tag{1.4}$$

The comma denotes differentiation with respect to the coordinate x^μ so that $f_{,\mu} \equiv \partial f / \partial x^\mu$. The Christoffels are used to construct a measure of curvature called the Ricci tensor:

$$R_{\mu\nu} = \Gamma^\alpha_{\mu\nu,\alpha} - \Gamma^\alpha_{\mu\alpha,\nu} + \Gamma^\alpha_{\beta\alpha}\Gamma^\beta_{\mu\nu} - \Gamma^\alpha_{\beta\nu}\Gamma^\beta_{\nu\alpha} , \tag{1.5}$$

and its contraction or trace, $R = g^{\mu\nu} R_{\nu\mu}$, known as the Ricci scalar.

This construction communicates the presence of spacetime geometry whereas the stress-energy tensor T describes the matter and energy content of the Universe. In practice, a symmetric Einstein tensor G satisfying special properties (i.e. the Bianchi identities given by $\nabla_\mu G^{\mu\nu} = 0$) is hand-picked to mirror the physical properties of the stress-energy tensor T (i.e. conservation laws derived from $\nabla_\mu T^{\mu\nu} = 0$). The final results needed for relativistic cosmology are the deduced Einstein equations themselves:

$$G_{\mu\nu} \equiv R_{\mu\nu} - \frac{1}{2} g_{\mu\nu} R = \frac{8\pi G}{c^4} T_{\mu\nu} . \tag{1.6}$$

Note that cosmologists tend to use units where the speed of light and the gravitational constant simplify the equations so that $c = 8\pi G = 1$. Equation 1.6 simply relates the fact that 'matter tells space how to curve, and space tells matter how to move.'

1.3.3 The Lambda-Cold Dark Matter (ΛCDM) model

The *Friedmann equations* of cosmology are deduced by assuming a perfect fluid embedded in the FRW spacetime of Eq. 1.1. The stress-energy tensor for a perfect fluid with energy density ρ and pressure p in a comoving reference frame of $u^\mu = dx^\mu / d\tau = (1,0,0,0)$ (i.e. spatial coordinates

Parameter	w	$\rho(a)$	Parameter	w	$\rho(a)$
Ω_Λ	-1	a^0	Ω_m, Ω_b	0	a^{-3}
Ω_k	—	a^{-2}	Ω_γ, Ω_ν	$\frac{1}{3}$	a^{-4}

Table 1.1 The equation of state $w \equiv p/\rho$ and corresponding energy density dependence $\rho \propto a^{-3(1+w)}$. The parameter contributions correspond to dark energy Ω_Λ, curvature Ω_k, cold dark matter Ω_m, baryons Ω_b, photons Ω_γ, and neutrinos Ω_ν.

remain fixed in the expanding spacetime) is

$$\begin{aligned} T^\mu_\nu &= g^{\mu\sigma} T_{\sigma\nu} = (\rho + p)\, u^\mu u_\nu - p\delta^\mu_\nu \\ &= \mathrm{diag}(\rho, -p, -p, -p)\,. \end{aligned} \tag{1.7}$$

Therefore, putting the left and right hand sides of the Einstein equations together (see Eq. 1.6) the general Friedmann equations for flat space are [21]:

$$H^2 \equiv \left(\frac{da/dt}{a}\right)^2 = \frac{\rho}{3} \quad \text{and} \quad \frac{dH}{dt} + H^2 = -\frac{\rho + 3p}{6}\,. \tag{1.8}$$

We have associated a derivative of the scale factor with the Hubble constant so that relativity connects directly with observation. Fundamentally, the Hubble parameter may be visualized as the proper velocity of the scale factor (i.e. $H = da/d\tau = (da/dt)/a$ where t is the usual cosmic time and τ is the proper time in the FRW spacetime). At this point we combine the two parts of Eq. 1.8 to reduce them to a single continuity equation

$$\frac{d\rho}{dt} + 3H(\rho + p) = 0\,. \tag{1.9}$$

This is done in an effort to extract a simple yet realistic model for the Universe.

The Lambda-Cold Dark Matter (ΛCDM) model makes the assumption that the pressure p and the energy density ρ are proportional to each other. This simplifies the Friedmann continuity equation by distinguishing the contributions of various types of matter and energy. Thus, we may use the equation of state parameter $w \equiv p/\rho$ to solve Eq. 1.9 as

$$\rho \propto a^{-3(1+w)}\,. \tag{1.10}$$

The ΛCDM model is very flexible and allows the total energy density to be comprised of matter with different equations of state. Table 1.1 provides a summary of these solutions under different forms of energy. For example, from statistical mechanics the equation of state is known to be $\rho = 3p$ so the energy density scales as a^{-4}. For all contributions in this model we define the total energy density as $\rho \equiv \sum \rho_i$ and the total pressure as $p \equiv \sum p_i$ so that the total equation of state is given by $w_i \equiv p_i/\rho_i$. Furthermore, for each component it is useful to define the ratio of the present energy density to the critical energy density ρ_{cr},

$$\Omega_i \equiv \frac{\rho_i}{\rho_{cr}} \quad \text{where} \quad \rho_{cr} \equiv \frac{3H_0^2}{8\pi G}. \tag{1.11}$$

Note that we could affix a subscript "0" to signify the present value so that the Hubble constant H_0 is the present value of the Hubble parameter H. Under this final simplification Eq. 1.8 reduces to the compact statement

$$\frac{H^2(t)}{H_0^2} = \frac{\rho}{\rho_{cr}} = \sum_i \frac{\rho_i}{\rho_{cr}}. \tag{1.12}$$

The ΛCDM parameter space allows for many different types of universes, however, the point of the model is to find the one that matches the Universe in which we live. A surprisingly simple but accurate description is given by assuming only dark energy with $\Omega_\Lambda \sim 0.7$ and cold dark matter with $\Omega_m \sim 0.3$. To emphasize the simplicity we take Eq. 1.12 to a final explicit equation for the Hubble parameter as a function of the redshift factor $z = 1/a - 1$

$$H(z) = H_0\sqrt{\Omega_\Lambda + \Omega_m(z+1)^3}. \tag{1.13}$$

Finally, we note that the ΛCDM model is easily extended to include contributions from curvature Ω_k, photons Ω_γ, neutrinos Ω_ν, and baryons Ω_b. A summary of equations of state w_i and densities $\rho_i(a)$ for the most common energy contributions may be found in Table 1.1.

1.3.4 Parameter constraints

The ΛCDM model assumes isotropy so it needs to be extended in order to infer parameter constraints from the anisotropic CMB. However, as stated above the simple model is a surprisingly good approximation to our Universe on large scales. Thus, the next step is to assume small perturbations on top of the original solutions. The perturbations need to be inserted into all sources of anisotropy; including the metric, the temperature, and matter densities. It turns out that these equations cannot be solved exactly so we rely on numerical calculations for the results of Chapter **??**. However, we now introduce the connection between these perturbative effects.

The early Universe consisted of a dense cosmic plasma with small deviations from an equilibrium state. The study of nonequilibrium mechanics is considerably more complicated than what is taught in an introductory thermodynamics course but basic ideas are extensions of familiar concepts. The formulation is based on the Boltzmann equation, which consists of an integrodifferential equation over the phase space (See Ref. [20] for details). The essential idea is to relate the change in a distribution f to the physical and state variables (x and p respectively) via the chain rule

$$\frac{df}{dt} = \frac{\partial f}{\partial t} + \frac{\partial f}{\partial x^i} \cdot \frac{dx^i}{dt} + \frac{\partial f}{\partial p^i} \cdot \frac{dp^i}{dt} = C[f]\,. \tag{1.14}$$

$C[f]$ is a "collision integral" equal to zero under equilibrium conditions but nonzero for scattering, absorption, nuclear reactions, pair production, etc. Throughout this section we use p^i for the phase space momentum E_i for the energy components. We now integrate Eq. 1.14 over the distribution f_j to get a relation for the scaled number density n_j. For the case of Big Bang nucleosynthesis (BBN) we leave some of the details as words in order to bring out the physics. For a species j in an expanding universe the result is given by

$$a^{-3}\frac{d(n_j a^3)}{dt} = \prod_{i=1}^{N} \int \frac{d^3 p_i}{(2\pi)^3 2E_i} \times (\text{Conservation Laws}) \times (\text{BBN Reactions})\,. \tag{1.15}$$

This allows for analytic progress in modeling changes in the composition of the Universe during events such as BBN.

The front ends of equations such as Eq. 1.14 are tedious to keep writing down so we work with unintegrated equations for cosmological perturbations. Also we must use the explicit form of the linearized anisotropic metric

$$ds^2 = -(1+2\Psi(\vec{x},t))dt^2 + a^2(1+2\Phi(\vec{x},t))(dx^2+dy^2+dz^2)\,, \tag{1.16}$$

which is the extension of Eq. 1.2. Mathematically, the perturbative corrections allow for relations between overdensities in the early Universe (i.e. geometry Φ and Ψ, matter ρ, and temperature Θ). The simplified calculation leaves the following for the left hand side of Eq. 1.14:

$$\frac{df}{dt} = \frac{\partial f}{\partial t} + \frac{p^i}{a}\frac{\partial f}{\partial x^i} - p\frac{\partial f}{\partial p}\left[H + \frac{\partial \Phi}{\partial t} + \frac{p^i}{a}\frac{\partial \Psi}{\partial x^i}\right]. \tag{1.17}$$

This is the general starting point because various types of matter will have different distributions f and different collision integrals $C[f]$. For example, for dark matter we expect very little interaction with other types of matter, but this is not the case with baryons. We may continue to make analytic progress with the Boltzmann equations by considering the evolution of a species under nonequilibrium conditions. We now do so with photons.

Fluctuations in the CMB are encoded in perturbative corrections to the distribution of photons under the Boltzmann equation. To zeroth order photons follow the Bose-Einstein distribution with zero chemical potential,

$$f^{(0)} \equiv \frac{1}{e^{p/T}-1}\,. \tag{1.18}$$

Recall that we are using units where $k_B = 1$. Thus, if we allow for a small correction to the original isotropic temperature $T(\vec{x},\hat{p},t) = T(t)[1+\Theta(\vec{x},\hat{p},t)]$ then a first order temperature expansion of the photon distribution is given by

$$\begin{aligned} f(\vec{x},p,\hat{p},\tau) &= \left[\exp\left\{\frac{p}{T(\tau)[1+\Theta(\vec{x},\hat{p},\tau)]}\right\} - 1\right]^{-1} \\ &\approx f^{(0)} - p\frac{\partial f^{(0)}}{\partial p}\Theta. \end{aligned} \tag{1.19}$$

The zeroth order homogeneous, isotropic equilibrium equation gives

$$\left.\frac{df}{dt}\right|_{\substack{\text{zeroth}\\ order}} = \frac{\partial f^{(0)}}{\partial t} - Hp\frac{\partial f^{(0)}}{\partial p} = 0\,, \tag{1.20}$$

with the important result that

$$T \propto \frac{1}{a}\,. \tag{1.21}$$

The first order equations relate additional physics for photons, dark matter, baryons, and other contributions with a nonzero collision integral $C[f]$. In essence this provides a set of three Boltzmann equations which complement the six Einstein equations. The linearized extensions of the zeroth order Einstein equations from Eq. 1.6 must also include corrections in Ψ, Φ, ρ, and Θ. In Chapter 2 we use a numerical approach to solving the Boltzmann-Einstein equations. This allows for the determination and analysis of cosmological parameters from CMB data.

1.4 Neutrino Physics

As nearly massless, neutral leptons, neutrinos interact weakly with other forms of matter at low energies. In fact, after the first second of expansion the Universe has cooled enough for neutrino decoupling to occur. After this time neutrinos maintain a Fermi–Dirac distribution with zero chemical potential and a temperature that falls inversely with the expanding scale factor, i.e. $T \propto a^{-1}$ [20]. In this section we investigate the properties of the effective neutrino number N_{eff} and the sum of the neutrino masses $\sum m_\nu$.

1.4.1 The effective neutrino number N_{eff}

The effective neutrino number N_{eff} is defined as the contribution of neutrinos to the relativistic degrees of freedom g_*. These degrees of freedom represent the effective number of relativistic particles in the early Universe and need not be an integer value. For example, in a standard physics

scenario the particles contributing to the total value of $g_* \simeq 10.75$ are electrons, three neutrinos, three antineutrinos, and photons. Any extra relativistic degrees of freedom can be parameterized in terms of an excess with respect to the standard effective neutrino number $N_{eff} = 3$ (which, more precisely, is $\simeq 3.046$ after accounting for QED corrections and non-instantaneous decoupling of neutrinos) [28,29]. We will need the neutrino energy density ρ_ν for a later calculation. The density ρ_ν is in fact proportional to the energy density of photons ρ_γ through the number of neutrino generations N_{eff} by the relation

$$\rho_\nu = N_{eff} \frac{7}{8} \left(\frac{4}{11}\right)^{4/3} \rho_\gamma. \tag{1.22}$$

The factor of $7/8$ is due to the fact that neutrinos are fermions and photons are bosons. The factor of $(4/11)^{4/3}$ is included because photons are heated by e^+e^- annihilation. The main point is that ρ_ν is proportional to ρ_γ through the N_{eff} parameter.

One effect that N_{eff} can have is related to the primordial helium abundance Y_P. According to the standard picture of Big Bang nucleosynthesis (BBN), at a temperature of ~ 0.6 MeV all available neutrons are used to form helium. Thus, the helium abundance Y_P is approximately

$$Y_P \simeq \left.\frac{2n_n/n_p}{1+n_n/n_p}\right|_{T\simeq 0.6\text{ MeV}}, \tag{1.23}$$

which is determined by the value of n_n/n_p when the Universe reaches the freeze-out temperature T_{freeze}. The neutron to proton ratio remains roughly constant from then on, unless we consider neutron to proton decay. However, with a neutron half-life of about 15 minutes, the time-scale for this process is too long to affect n_n/n_p over the period in which BBN takes place. The helium abundance depends on g_* (and hence on N_{eff}) via the relation $T_{freeze} \simeq \frac{1}{2} g_*^{1/6}$, so larger g_* means earlier n_n/n_p freeze-out.

Finally, as Eq. 1.22 relates the neutrino energy density ρ_ν to the photon energy density ρ_γ we derive the latter for use in Chapter 2. The temperature of CMB photons has been measured at $T = 2.725 \pm 0.002$K by the COBE satellite (see Fig. 1.2). Thus, if photons have a Bose–Einstein

distribution f_{BE} with zero chemical potential, degeneracy g from two spin states, and phase space momentum p, then the energy density ρ_γ is [20]

$$\begin{aligned}\rho_\gamma &= \int \frac{g\, f_{BE}\, p\, d\mathrm{V}}{\text{Phase Volume}} \\ &= 2\int \frac{d^3p}{(2\pi)^3}\frac{p}{e^{p/T}-1}\,.\end{aligned} \tag{1.24}$$

The integral may be evaluated exactly with the substitution $x = p/T$ and knowledge of the Riemann zeta function ζ (i.e. $\zeta(4) = \pi^4/90$ and $\Gamma(4) = 3!$). The phase space is isotropic so we may immediately include a factor of $4\pi p^2$ for the angular part. The integration proceeds as follows:

$$\begin{aligned}\rho_\gamma &= \frac{8\pi T^4}{(2\pi)^3}\int_0^\infty \frac{x^3}{e^x-1}dx \\ &= \frac{T^4}{\pi^2}\Gamma(4)\,\zeta(4) \\ &= \frac{\pi^2}{15}T^4\,.\end{aligned} \tag{1.25}$$

However, the temperature in an expanding FRW spacetime is inversely proportional to the scale factor (See Eq. 1.21 and Table 1.1). Therefore, with a present temperature T_0 and scale factor a_0 the temperature history of photons is $T = T_0 a_0/a = 2.275\mathrm{K}/a$. Furthermore, with the critical density ρ_{cr} defined by Eq. 1.11 and the Hubble constant H_0 parameterized by a dimensionless quantity h, defined by

$$\begin{aligned}H_0 &= 100h\ \mathrm{km\ sec^{-1}\ Mpc^{-1}} \\ &= 2.133\times10^{-33}\ h\ \mathrm{eV}/\hbar\,,\end{aligned} \tag{1.26}$$

the contribution of photons to the total energy density Ω_γ is [20]

$$\begin{aligned}\Omega_\gamma \equiv \frac{\rho_\gamma}{\rho_{cr}} &= \frac{\pi^2}{15}T^4\frac{8\pi G}{3H_0^2} \\ &= \frac{\pi^2}{15}\left(\frac{2.725K}{a}\right)^4\frac{1}{8.098\times10^{-11}h^2\mathrm{eV}^4} \\ &= \frac{2.47\times10^{-5}}{h^2a^4}\,.\end{aligned} \tag{1.27}$$

The last line was calculated by inserting four factors of the Boltzmann constant (i.e. $k_B = 1$ implies $1\text{eV} = 11605\text{K}$). This stands to emphasize that although radiation was dominant in the early Universe ($a \ll 1$), we are justified in neglecting the contribution at late times.

1.4.2 The sum of the neutrino masses $\sum m_\nu$

We conclude this section by stating our purpose to further constrain the neutrino mass $\sum m_\nu$ and investigate any correlation with curvature Ω_k. The fact that neutrinos have mass to begin with is a relatively recent discovery. It was just over a decade ago when the experiment at Super–Kamiokande led to the general acceptance of neutrino mass [30]. Around the same time, the DONUT collaboration obtained the first detection of the tau neutrino species [31]. Since then the number of phenomenological questions regarding neutrinos has only increased.

Cosmology hopes to distinguish between two types of hierarchical models: a normal hierarchy with two "smaller" neutrinos and one "larger" neutrino, and an inverted hierarchy with one "smaller" neutrino and two "larger" neutrinos. Specifically, the models are distinguished by the arrangement of the absolute difference in the mass eigenstates. This is important because particle models with massive neutrinos are silent on whether there are *one* or *two* light neutrinos. At this point many particle physicists hope to learn more about this question from direct cosmological measurements. In fact, the different hierarchies may be distinguished by their effect on the matter power spectrum, but this may have to wait for the accuracy of future CMB experiments [32, 33]. Perhaps the upcoming Planck results will be sufficient to determine the neutrino hierarchy, however, high statistical significance may require additional experiments (See Fig. 1.4). Keep in mind that the CMB test is derived (not empirical) because it provides an upper bound on $\sum M_\nu$ through the fractional energy density $f_\nu \equiv \Omega_\nu/\Omega_m$ [34]. For information about how to extract $\sum m_\nu$ from f_ν see the discussion surrounding Eq. 2.24 in Section 2.3.2 regarding the code implementation.

With every major improvement in experimental cosmology it is important to analyze the current

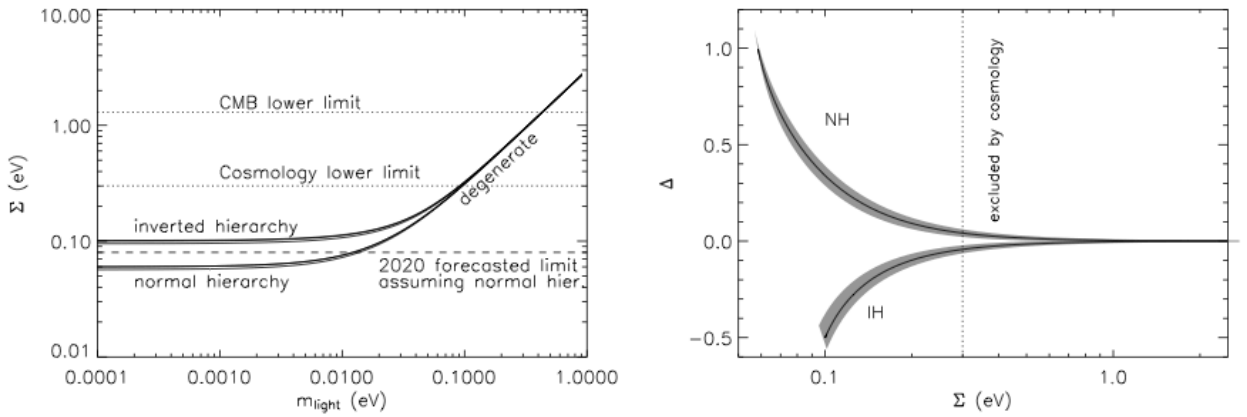

Figure 1.4 Constraints on the sum of the neutrino masses $\sum m_\nu$ based on projections of future experiments. The normal and inverted neutrino hierarchies diverge if $\sum m_\nu$ is small. Figure from Ref. [34].

status and direction of significant questions in physics. We hope that preference toward a particular hierarchical model may slightly improve with the combination of ACT and SPT datasets, however, a cosmological determination of the neutrino mass hierarchy largely remains a task for future experiments. Our contribution relates to the understanding of extended cosmological parameter spaces. Section 3.2 contains details about the connections between mass and curvature. Fig. 1.4 shows the projected constraints on $\sum m_\nu$ based on the mass differences. Future experiments should be able to constrain the mass accurately enough to favor either the normal or inverted hierarchy. However, when this level of precision is reached it will still be important to consider the effects that extended parameter spaces have on mass. A non-exhaustive list of additional references on the subject of constraining neutrino parameters includes Refs. [32–45].

1.5 Review and overview

The material from this chapter is designed to consolidate a variety of resources from the literature at the undergraduate level. This research began while I was a visiting student researcher for Asan-

tha Cooray at the University of California, Irvine and was completed at Brigham Young University with collaborators from the Universita' di Roma "La Sapienza." Students with similar interests should be directed by their advisors for the computational analysis of CMB data; however, the material presented in the remainder of the thesis may serve as a practical guide for research in this area of cosmology. So far we have provided an introduction to modern cosmology with the following question in mind: "What are the implications of failing to consider curvature in cosmological models involving neutrinos?" Thus, Chapter 1 is general and later chapters become increasingly specialized. Specifically, Chapter 2 contains three important aspects of the project. First, we use an analytical approach to explain the theoretical origin for correlation. Second, we provide an explanation of the statistical methods behind the Monte Carlo Markov Chain (MCMC) procedure. We also include the mathematics of a harmonic decomposition of CMB data. Third, we walk through the specific implementation of the computational analysis using the most recent data available. Chapter 3 provides confidence contours demonstrating correlation in the parameter space, tables featuring the parameter constraints, and a discussion of the significance of assuming cosmological flatness for the neutrino parameters N_{eff} and $\sum m_\nu$.

Chapter 2

Methods of Analysis

Chapter 1 provided an introduction to the significant theoretical concepts needed for a modern understanding of CMB cosmology. The current chapter is divided into three sections that sequentially focus on the theoretical, statistical, and computational tools used in the thesis. Chapter 3 discusses the results of the computational aspects of constraining parameters. Thus, the scope and application of each chapter become increasingly directed toward the core investigation of how cosmological flatness affects neutrino properties.

2.1 Analytical methods

2.1.1 The sound horizon $r_s(N_{eff})$

Additional neutrino species influence the evolution of the early Universe. The effect of the number of neutrino species N_{eff} on cosmological observables (e.g. CMB anisotropy power spectrum) can be seen in considering when the epoch of matter-radiation equality a_{eq} occurred. This is the point in the Universe's history in which the energy distribution shifted from being dominated by radiation to being dominated by matter. In particular, increasing a_{eq} will change the extent of the

so-called integrated Sachs-Wolfe (ISW) effect [46]. The early ISW effect changes the distribution of temperature hotspots. In analogy with classical potential wells, the radiation collects in areas of greatest "depth," the imprint of which may be seen in the CMB. The ISW effect is essentially the same mechanism that extracts energy from gravitationally lensed photons (i.e. the deflection of starlight by massive objects). At this point neutrinos act as an additional source of radiation, so a larger number of neutrino species N_{eff} pushes a_{eq} to a later time. In turn, this would increase the amount of radiation trapped in these potential structures before their eventual escape and observation via the CMB. The decoupling of this increased radiation from the potential structures will have a noticeable effect on CMB anisotropy measurements.

The particular relation between a_{eq} and N_{eff} is given by equating the matter and radiation energy densities we presented in Section 1.3.3 (Specifically Eq. 1.11 and Table 1.1):

$$\rho_m = \rho_{rad} \tag{2.1}$$

$$\Omega_m a_{eq}^{-3} = (\Omega_\gamma + \Omega_\nu) a_{eq}^{-4} . \tag{2.2}$$

At this point we incorporate Eq. 1.22 to write Ω_ν in terms of Ω_γ and Eq. 1.27 to give the currently observed value Ω_γ. The epoch of equality is given by

$$\begin{aligned} a_{eq} &= \frac{\Omega_\gamma}{\Omega_m}\left[1 + N_{eff}\frac{7}{8}\left(\frac{4}{11}\right)^{4/3}\right] \\ &= \frac{1 + 0.22711 N_{eff}}{40484\,\Omega_m h^2} . \end{aligned} \tag{2.3}$$

The calculations in this section are used to provide a qualitative description of correlation between the curvature Ω_k and the effective neutrino number N_{eff}, so the precision of numbers is arbitrary and chosen by the author for compactness and readability.

The epoch of matter-radiation equality a_{eq} is linear in N_{eff} (Eq. 2.3 results from the approximation in Eq. 2.1), which is important because many cosmological observables are influenced by a_{eq}. At the end of this calculation we will reveal a series of "Russian doll" dependences to reach

an observable related to curvature. In particular, the dependence transfers directly to the baryon to photon ratio R. The ratio at equality R_{eq} is given by [20]:

$$\begin{aligned} R_{eq} &\equiv \frac{3\rho_b}{4\rho_\gamma}\Big|_{a_{eq}} \\ &= 30496\,\Omega_b h^2 a\Big|_{a_{eq}} \\ &= \frac{1+0.22711N_{eff}}{1.3276}\frac{\Omega_b}{\Omega_m}. \end{aligned} \tag{2.4}$$

The presence of baryons in the relativistic cosmic fluid slows down the sound speed c_s by the factor

$$c_s \equiv 1/\sqrt{3(1+R)}, \tag{2.5}$$

and so this quantity also depends on N_{eff} at equality. This is ultimately reflected in the size of the so-called sound horizon r_s at a generic time τ. The sound horizon is the comoving distance traveled by a sound wave in the time τ. Said another way it is just the integrated sound speed c_s. Note: Comoving distances simply move with the expanding spacetime so that stationary objects remain at fixed coordinates. This is already taken care of when the time component is *proper* or *conformal*. In the context of Eq. 1.2 the proper time τ is related to the metric time t via $dt = a\,d\tau$. We are interested in integrating with respect to the scale factor a, which may be done through the definition of the Hubble factor, or $H \equiv \frac{1}{a}\frac{da}{dt} \;\Rightarrow\; d\tau = \frac{da}{a^2 H}$ [20]. Therefore the sound horizon is

$$\begin{aligned} r_s &\equiv \int_0^\tau d\tau'\, c_s(\tau') \\ &= \int_0^a \frac{da}{a^2 H}\, c_s(a) \\ &\approx \frac{2}{3k_{eq}}\sqrt{\frac{6}{R_{eq}}}\ln\left\{\frac{\sqrt{1+R}+\sqrt{R+R_{eq}}}{1+\sqrt{R_{eq}}}\right\} \\ &= \frac{6.612\times10^{-3}}{H_0\sqrt{\Omega_m\Omega_b h^2}}\ln\left\{\frac{\sqrt{1+R}+\sqrt{R+R_{eq}}}{1+\sqrt{R_{eq}}}\right\}. \end{aligned} \tag{2.6}$$

The last two lines come from assuming the Universe is matter dominated during recombination. We consider typical values for the present Hubble constant H_0, the total matter contribution Ω_m,

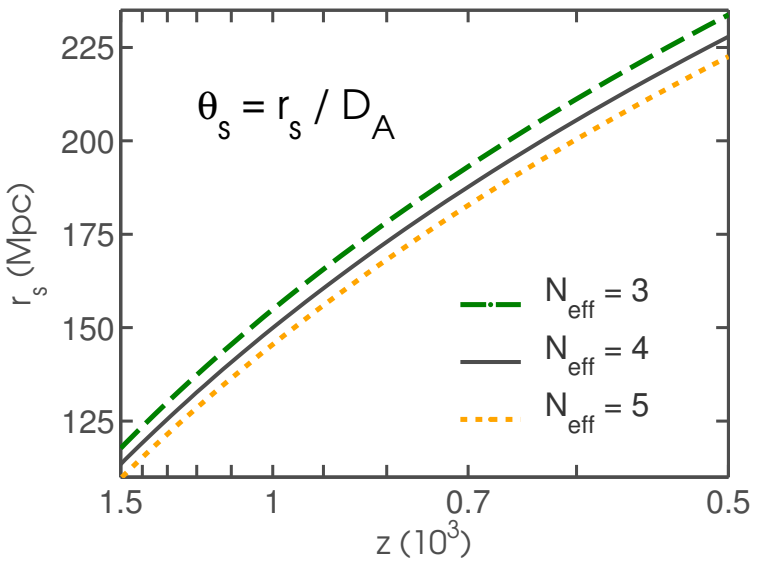

Figure 2.1 A demonstration of how the sound horizon r_s changes with the effective neutrino number N_{eff} under the matter dominated approximation of Eq. 2.6.

and the contribution from baryons Ω_b [11]. As can be seen in Fig. 2.1, the sound horizon r_s depends on N_{eff} through R_{eq}. The "Russian doll" dependence structure is as follows: the sound horizon r_s depends on the sound speed c_s, which depends on the baryon to photon ratio at equality R_{eq}, which in turn depends on the epoch of matter-radiation equality a_{eq}, which finally depends on N_{eff}!

In [2] the authors provide qualitative arguments for how changing the number of allowed neutrinos affects the observed values of parameters. One qualitative example which we use is the relative dependence of distance measurements on the Hubble constant. In fact, the sound horizon at recombination scales as $r_s \propto 1/H$ while the distance a photon typically diffuses prior to its last scattering goes as $r_d \propto 1/\sqrt{H}$. This is significant because the response of the radiation relative to matter determines the degree of damping prior to recombination θ_s. In other words, with $\theta_s = r_s/D_A$ fixed by observation, the angular diameter distance D_A must must also decrease as $1/H$, which is more rapid than r_d. Thus, the damping increases according to $\theta_d = r_d/D_A \propto \sqrt{H}$ [2]. If these distances depend on H then they similarly depend on various parameters correlated with H.

2.1.2 The angular diameter distance $D_A(\Omega_k)$

Distances are calculated by tracing radial light rays to the emission source. Geometrically, this is done by integrating along a null geodesic in the spherically symmetric spaces of constant curvature (k). The extension of the FRW metric (see Eq. 1.2) to include curvature is given by

$$ds^2 = -dt^2 + a(t)^2 \left(\frac{dr^2}{1-kr^2} + r^2 d\Omega^2 \right), \tag{2.7}$$

where $d\Omega^2 = d\theta^2 + \sin\theta d\phi^2$ is the differential element for the unit sphere in spherical coordinates. The null condition is $ds^2 = 0$ and the condition that our light rays be radial gives $d\Omega^2 = 0$. We can then rearrange the metric in Eq. 2.7 into the form

$$\frac{dt}{a(t)} = \frac{dr}{\sqrt{1-kr^2}}. \tag{2.8}$$

Equation 2.8 allows for the calculation of the comoving distance χ in terms of the angular diameter distance D_A (Note: The speed of light does not appear because we have set $c = 1$)

$$\chi \equiv \int_\tau^{\tau_0} d\tau' = \int_t^{t_0} \frac{dt'}{a(t')} = \int_0^{D_A} \frac{dr}{\sqrt{1-kr^2}}. \tag{2.9}$$

The integral depends on the sign of k, which is related to the cosmological parameter for curvature by $\Omega_k = -k/H_0^2$, where the Hubble Constant H_0 is the present value of the Hubble parameter. Solving for the angular diameter distance D_A after integrating Eq. 2.9 gives [20, 47]

$$D_A = \frac{a}{H_0\sqrt{|\Omega_k|}} \left\{ \begin{array}{ll} \sin[\sqrt{-\Omega_k} H_0 \chi] & \Omega_k < 0 \\ \sinh[\sqrt{\Omega_k} H_0 \chi] & \Omega_k > 0 \end{array} \right\}. \tag{2.10}$$

For a practical calculation of the comoving distance χ we use a change of variables to integrate with respect to the redshift factor $z = 1/a - 1$:

$$\chi(z) \equiv \int_\tau^{\tau_0} d\tau' = \int_a^1 \frac{da'}{a'^2 H(a')} = \int_0^z \frac{dz'}{H(z')}. \tag{2.11}$$

In this case we may use a ΛCDM model for $H(z)$ similar to Eq. 1.13 except with radiation and curvature included. For the case of a flat cosmology the angular diameter distance is related linearly with the comoving distance, so that $D_A = \chi/1+z$.

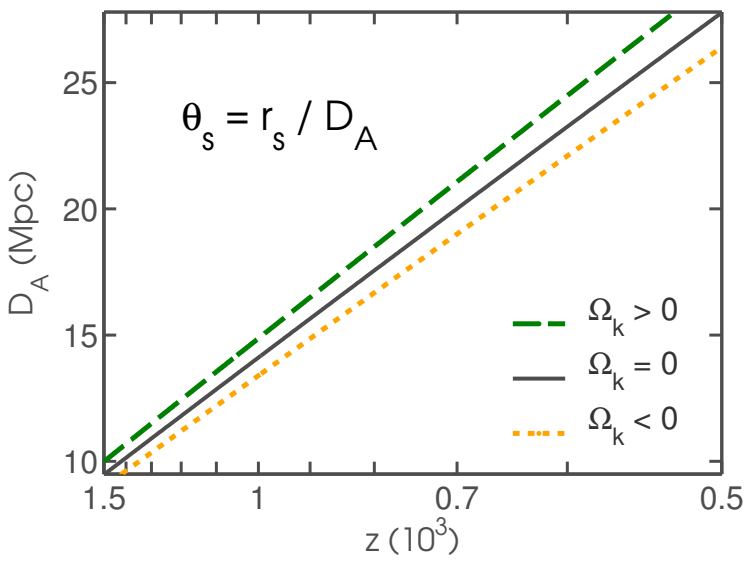

Figure 2.2 A demonstration of how the angular diameter distance D_A changes with curvature Ω_k under the ΛCDM model. The ratio of the sound horizon to the angular diameter distance determines the degree of damping prior to recombination θ_s, which is fixed by observation. Note: $\Omega_k \in (-0.025, 0.025)$.

Apparently, distances are larger in an open universe with nonzero curvature ($\Omega_k > 0$), as demonstrated by Fig. 2.2. Therefore by the argument directly preceding this section, in an open universe the effective neutrino number is slightly reduced. The theory confirms this because as stated above θ_s is constrained by observation which means if N_{eff} is reduced and $\Omega_k > 0$ then r_s and D_A both increase (see Fig. 2.1). However, if the parameter space favors a closed universe then there will appear to be a higher number of effective neutrinos. This is one of the primary reasons for expecting correlation between N_{eff} and Ω_k.

Much stronger correlation exists between Σm_ν and Ω_k. However, this is expected because massive neutrinos are still relativistic at decoupling so they act as additional radiation (c.f. Ref. [48]). As a consequence the presence of massive neutrinos shifts both the time of matter-radiation equality a_{eq} and the position of CMB peaks. This effect can be compensated for by a change in the geometry of the Universe, which weakens the constraints on both $\sum m_\nu$ and Ω_k (See Section 3.2).

2.2 Statistical methods

As the size of datasets gets considerably larger, cosmologist need fast and reliable statistics to evaluate various models. We review the fundamental principles of the Bayesian statistical framework and the various sources of error in CMB measurements. We also include a discussion on the mathematics behind CMB anisotropies to better understand the calculation of the power spectrum underlying the computational methods of Section 2.3.

2.2.1 Bayesian statistics

The human mind naturally works under a Bayesian framework because decisions are based on the information at hand combined with one's experience, or *prior* belief regarding the outcome of events. We emphasize this prior information because frequentist statisticians tend to avoid making assumptions, saying instead that probabilities are determined by a limit of independent trials. We use the Bayesian framework because we study the evolution of a unique Universe. The one observable trial we do have allows for the inference of parameter probability distributions described in further sections.

Realistic cosmological models usually have about a dozen parameters that are tuned to fit the experimental data. These parameters answer questions about quantities: how much of this, how fast is that, or what law does it follow? The lack of information about the model is contained within probability distributions $P(k)$ of continuous parameters k. These distributions are non-negative and normalized so that $\int P(k)dk = 1$. If data d is available, then we may realize a conditional probability $P(d|k_H)$ of the data given a particular model with hypothesis parameters k_H. Thus, the probability that both the model parameters and the data happen to be correct is given by [20, 49]

$$P(d \cap k_H) = P(d|k_H)P(k) \quad \text{and} \quad P(k_H \cap d) = P(k_H|d)P(d)\,. \tag{2.12}$$

Actually, the two parts of Eq. 2.12 are equal, which is the basis for Bayes theorem,

$$P(k_H|d) = \frac{P(k_H)P(d|k_H)}{P(d)}. \tag{2.13}$$

This is exactly the information we need to know! Bayes theorem gives a way to find the probability distribution that a theoretical model is correct given the experimental data. The names for the contributions to Eq. 2.13 are the *posterior* distribution $P(k_H|d)$, the prior distribution $P(k_H)$, and the likelihood function $P(d|k_H)$. The probability of the data $P(d)$ ends up being a normalizing constant, so the explicit form of Bayes theorem is

$$\text{Posterior} \propto \text{Prior} \cdot \text{Likelihood}. \tag{2.14}$$

The cosmological prior is an essential consideration with this kind of analysis. We will define the specific prior used for this thesis in Section 2.3.2, but for the moment note that as long as priors are fairly reasonable the large datasets we consider will provide a barrier that will protect from prior induced biases. We also note that Gonzalez Morales *et al.* have recently argued that the statistical prior is responsible for the entirety of the N_{eff} question [50]. This is an important consideration, however, the robustness of the computational analysis used by the majority of the CMB community engenders confidence in our methods.

The Monte Carlo Markov Chain (MCMC) analysis that we will present in Section 2.3 is based on this Bayesian framework. It is difficult to directly draw from $P(k_H|d)$, however, we may construct the distribution using an iterative process that generates the desired draws, i.e. a ratio that gives samples in the correct proportions. This is done by setting up a random walk over the parameter space k_H that preferentially samples regions of high probability. The random walk is the "Monte Carlo" part of the algorithm and the way the walk samples is the "Markov Chain" part of the algorithm. This is given by $Q(k_{H,t+1}|k_{H,t})$, or the transition probability of moving from $k_{H,t}$ to $k_{H,t+1}$, which depends only on the current configuration $k_{H,t}$. The samples will have a probability density function equal to $P(k_H|d)$ because the next step is considered and accepted with a prob-

ability based on substituting the ratio of proposed and previous values of Eqs. 2.13 or 2.14. The exact method is given by iterating between the following steps:

1. Propose a new value $k_{\rm prop}$ for $k_{H,t+1}$, taken from the distribution $Q(k_{\rm prop}|k_{H,t})$, which is often a multivariate Gaussian with mean X_t or a top hat prior as shown in Fig. 2.4. It is usually better to have the distribution pick points that are nearby in the parameter space.

2. Decide whether to accept the proposed value based on the ratio

$$r = \frac{P(k_{\rm prop}|d)}{P(k_{H,t}|d)} \frac{Q(k_{H,t}|k_{\rm prop})}{Q(k_{\rm prop}|k_{H,t})}. \tag{2.15}$$

   If $r \geq 1$ then we accept the transition and set $X_{t+1} = k_{\rm prop}$. If $r < 1$ we only accept $k_{\rm prop}$ with a probability of r. If $k_{\rm prop}$ is rejected then $X_{t+1} = X_t$.

In practice, we allow for a "burn in" period to alleviate skewed contributions from the initial configurations (i.e. depending on the analysis we throw away the first 100 or even 100,000 draws). Thus, with many chains, or MCMC processes, we may be confident in converging on a reliable posterior distribution.

In order to calculate the statistical properties of a given parameter we *marginalize*, or numerically integrate, over all other parameters. The idea behind this is that if we are in a multidimensional parameter space we can project onto an axis via $P(k_1) = \int P(k1, k2, \ldots, k_n) dk_2 \cdots dk_n$. We may also arrive at a two dimensional probability distribution by marginalizing over all but two parameters in the parameter space. This allows for intuitive contour plots similar to Fig. 3.1 that provide qualitative and quantitative descriptions of correlation between the parameters. The apparent correlation revealed in these plots may either be due to fundamental physics or an artifact of the particular model. We return to the topic of parameter interpretation in Chapter 3.

2.2.2 The mathematics of CMB anisotropies

The power spectrum $P(k)$ of the CMB cab be thought of as a measure of how much the background blackbody radiation deviates from strict isotropy. If the CMB were perfectly isotopic $P(k)$ would be a constant. It is, of course, not a constant and $P(k)$ is then a measure of how far the radiation is from being a pure blackbody. A clever way to talk about fluctuations at various length scales is to decompose the data into harmonic space, where low ℓ modes correspond to differences on large scales and high ℓ modes refer to smaller scales. Recall that the central limit theorem tells us that large statistical samples will give rise to Gaussian distributions. To a good approximation the distribution of density fluctuations $\delta = \delta\rho/\rho$ (called the *overdensity* because it gives the relative change in the distribution or identifies regions of varying density) from the early Universe can be considered to be roughly Gaussian. Gaussian fields are special because they can be completely specified by a two point correlation function ξ (i.e. a comparison between how much two points differ from each other on various scales is enough to specify distribution). In fact, the two point correlation function ξ is directly related to the power spectrum $P(k)$ through the Fourier transform and is given by

$$\begin{aligned}\xi(\vec{x}-\vec{x}') &\equiv \langle \delta(\vec{x})\delta(\vec{x}')\rangle \\ &= \int \frac{d^3k}{(2\pi)^3} P(k) e^{i\vec{k}\cdot(\vec{x}-\vec{x}')}. \end{aligned} \tag{2.16}$$

It is common for cosmologists to use the Fourier convention of $f(\vec{x}) = (2\pi)^{-3}\int d^3k\, f(\vec{k})\exp\{i\vec{k}\cdot\vec{x}\}$ and $f(\vec{k}) = d^3x \int f(\vec{x})\exp\{-i\vec{k}\cdot\vec{x}\}$. The $\langle\cdots\rangle$ averaging is over all realizations of the density field. Thus, the power spectrum is given by

$$P(k) = \int d^3x\, \xi(\vec{x}) e^{-i\vec{k}\cdot\vec{x}}. \tag{2.17}$$

We note that non-Gaussian distributions need higher order correlation functions and corresponding higher order spectral descriptions (e.g. a bispectrum compares information from three points and

their two independent connecting length scales). The study of how non-Gaussian affects the CMB requires keeping track of algebra consisting of Wigner 3-j symbols and implementations of Wick's theorem. We do not discuss this further.

Finally, we make specific contact to the harmonic decomposition of the CMB. Recall from the first order temperature deviation in the Bose-Einstein photon distribution of Eq. 1.19 that $T(\vec{x},\hat{p},\tau) = T(\tau)[1+\Theta(\vec{x},\hat{p},\tau)]$ The temperature overdensity Θ is only observed today (at τ_0) and is averaged over spherical harmonics to encode the (2D) CMB information. Thus, the decomposition gives [20]

$$\Theta(\vec{x},\hat{p},\tau) = \sum_{l=1}^{\infty}\sum_{m=-l}^{l} a_{lm}(\vec{x},\tau)Y_{lm}(\hat{p})\,, \tag{2.18}$$

where the property of orthogonal harmonics (i.e. $\int d\Omega Y_{lm}(\hat{p})Y^*_{l'm'}(\hat{p}) = \delta_{lm}\delta_{l'm'}$) uniquely determines the coefficients through the relation

$$a_{lm}(\vec{x},\tau) = \int \frac{d3k}{(2\pi)^3}\, e^{i\vec{k}\cdot\vec{x}} \int d\Omega Y^*_{lm}(\hat{p})\Theta(\vec{x},\hat{p},\tau)\,. \tag{2.19}$$

Each a_{lm} is drawn from the same distribution with variance C_l determined by $\langle a_{lm}a^*_{l'm'}\rangle = \delta_{lm}\delta_{l'm'}C_l$. However, there is a fundamental uncertainty called *cosmic variance* that limits knowledge about the low mode C_ls according to

$$\Delta C_l = \sqrt{\frac{2}{2l+1}}\,C_l\,. \tag{2.20}$$

This is why the plotted power spectra of Fig. 2.3, which is plotted in terms of $\ell(\ell+1)C_\ell/2\pi$ [μK^2], has large uncertainty for low ℓ modes. Also when the temperature fluctuation map is plotted in Fig. 2.3 the WMAP team has subtracted out the low ℓ modes because the monopole is the average temperature and the dipole corresponds to differences resulting from the motion of our local galaxy. Finally, a calculation similar to that of Eq. 2.16 relates the C_l to the matter power spectrum $P(k)$. This is because the ratio of the temperature Θ and matter δ overdensities has nice properties arising from the perturbation equations of Subsection 1.3.4. Qualitatively, the correlation functions are

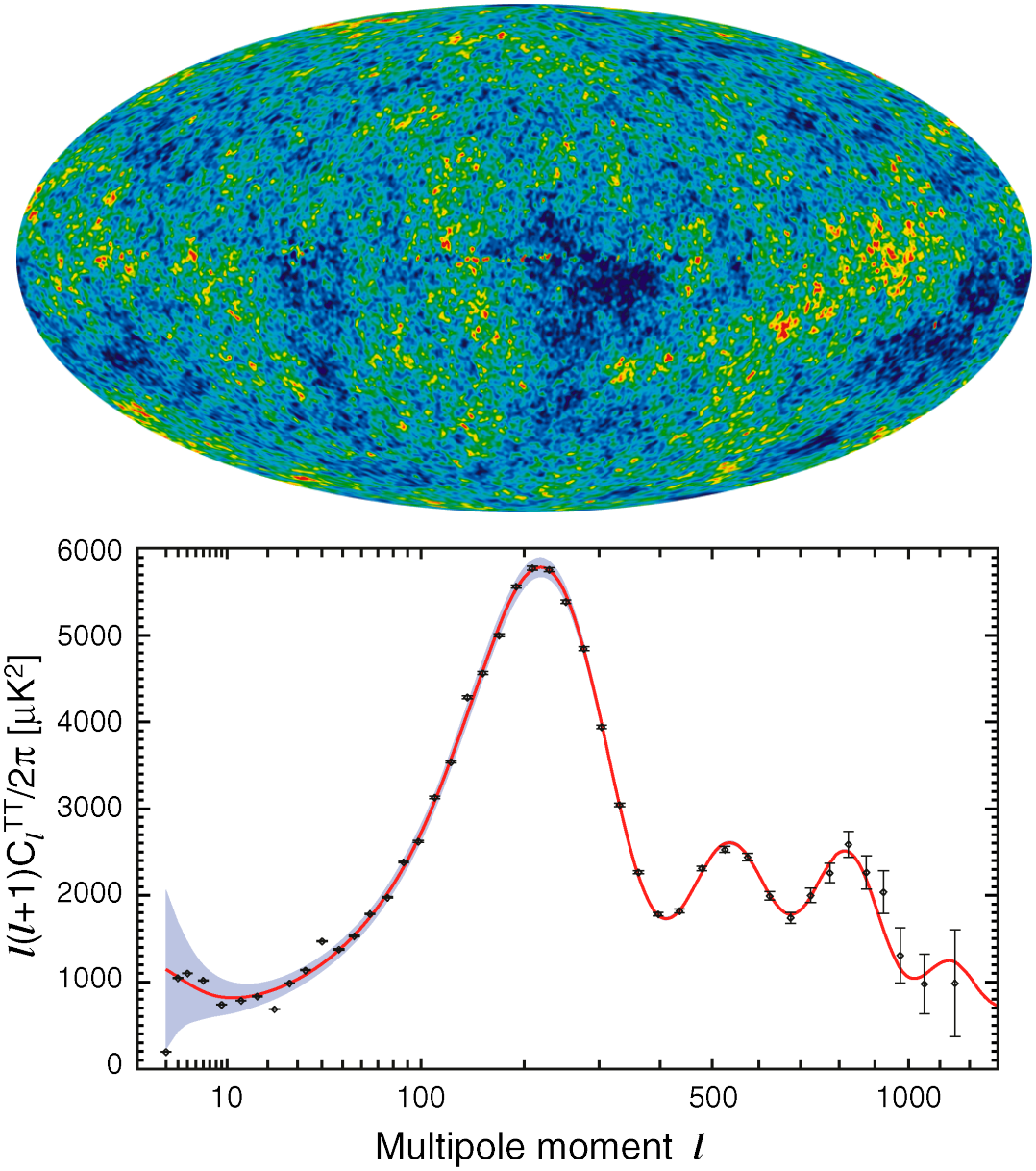

Figure 2.3 The first image is the internal linear combination sky map from WMAP 7-year observations. The temperature fluctuations are shown with subtractions of the monopole (average tempurature), dipole (from the motion of our local galaxy), and the excess radiation from the plane of the Milky Way. The image is also shown using data from multiple bandwidths. The second image is a plot of the corresponding TT matter power spectrum. Notice the uncertainty from cosmic variance with low ℓ modes. The plot is given in terms of $\ell(\ell+1)C_\ell/2\pi$ [μK^2]. Figure from Ref. [51].

related via

$$\langle \Theta\Theta \rangle = \langle \delta\delta \rangle \frac{\Theta}{\delta}\frac{\Theta}{\delta}, \tag{2.21}$$

so that the spectral relation is given by

$$C_l = \frac{2}{\pi}\int_0^\infty dk\, k^2\, P(k) \left|\frac{\Theta_l(k)}{\delta(k)}\right|^2, \tag{2.22}$$

where this provides *most of* the information to plot the curve in Fig. 2.3. This is a rich subject which merits considerable discussion on its own (see e.g. Ref. [10]).

2.3 Computational analysis

2.3.1 Specialized code: CosmoMC

In order to fit cosmological models to data we use a modified version of the publicly available CosmoMC software package [52]. This uses a Monte Carlo Markov Chain analysis on calculations of the lensed CMB power spectrum made with the fast Boltzmann code CAMB (Code for Anisotropies in the Microwave Background) package [53]. The FORTRAN90 code is designed to be as fast and accurate as possible given the large datasets used in cosmology. This relates back to Subsection 1.3.4 about Boltzmann equations because the full numerical solutions are considered when constructing the likelihood function. Models with different parameter distributions are run through the Bayesian sampling framework until the "chains" converge to a particular distribution. We use a convergence diagnostic test known as the "$R-1$" statistic which relates the chain means to the mean of variances. Usually, a convergence of $R-1 < 0.01$ is more than adequate for CMB parameters [49]. With three nodes of eight processors each the computation of a fiducial cosmology is completed in an afternoon. Once additional datasets and parameters are included the process may take up to a week. Luckily, the progress and preliminary results may be monitored throughout.

Parameter	WMAP+BAO+H_0	WMAP+SPT	WMAP+ACT	WMAP+SPT+ACT
$100\Omega_b h^2$	2.249 ± 0.054	2.256 ± 0.041	2.235 ± 0.047	2.258 ± 0.040
$\Omega_c h^2$	0.135 ± 0.016	0.130 ± 0.0094	0.137 ± 0.012	0.129 ± 0.0091
Ω_Λ	0.721 ± 0.018	0.722 ± 0.015	0.714 ± 0.018	0.722 ± 0.015
n_s	0.979 ± 0.015	0.9808 ± 0.0122	0.982 ± 0.013	0.9803 ± 0.0121
τ	0.086 ± 0.014	0.085 ± 0.014	0.086 ± 0.014	0.086 ± 0.014
H_0(km/s/Mpc)	75.1 ± 3.4	74.0 ± 2.0	74.6 ± 2.15	73.9 ± 1.92
N_{eff}	4.34 ± 0.88	3.91 ± 0.43	4.30 ± 0.58	3.89 ± 0.41

Table 2.1 Summary of matching results from WMAP 7-year [11], SPT [12], and ACT [13]. Note that the analyses are modeled by the choice to reproduce SPT results, which produces a smaller value for N_{eff} than expected for ACT data. All datasets include BAO and H_0 for improved parameter constraints. The quoted errors are given at the 68% confidence levels (CL).

Our MCMC analysis combines the following CMB anisotropy datasets: WMAP 7-year [11], SPT [12], and ACT [13]. Including BAO+H_0 simply means we are using the baryon acoustic oscillation (BAO) data of Percival *et al.* [54] and impose a prior on the Hubble parameter based on the last Hubble Space Telescope observations [55]. We integrate spectral data out to $\ell_{\max} = 3000$. We sample from the following parameters: the baryon $\Omega_b h^2$, cold dark matter $\Omega_c h^2$, and dark Ω_Λ energy densities, the scalar spectral index n_s, the optical depth to reionization τ, the Hubble parameter H_0, and the amplitude of SZ spectrum A_{SZ}. For the purposes of this analysis we also consider the effective neutrino number N_{eff}, spatial curvature Ω_k, and the sum of neutrino masses $\sum m_\nu$. Factors, such as degeneracy and poor choices for the parameter space, slow the rate of convergence and mixing of the chains. The first column in Table 2.1 provides a confirmation of the results in the literature using WMAP 7-year data, Baryon Acoustic Oscillations (BAO), and the Hubble Space Telescope (H_0) [11].

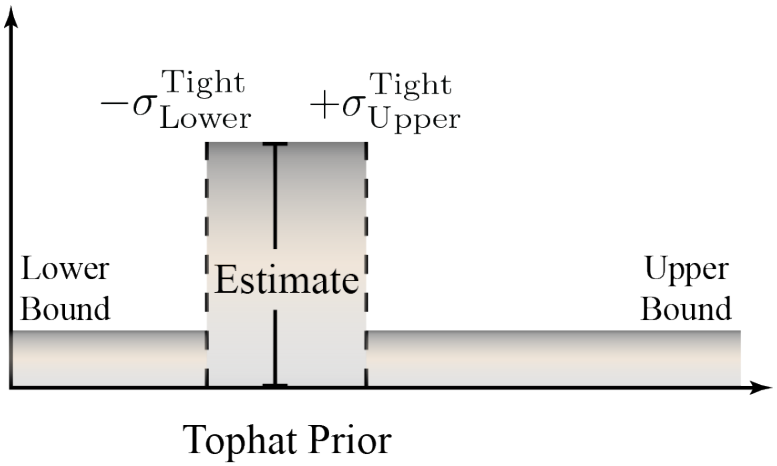

Figure 2.4 A visualization of a top hat prior distribution. The primary motivation for assuming such a distribution is the general improvement from a uniform distribution, which assumes no prior information. There are strict upper and lower bounds as well as a tighter best estimate based on the current understanding of the parameter. As an example, the notation of Eq. 2.23 places a prior of $N_{eff} \approx 3.04^{+0.5}_{-0.5} \in [0, 10]$.

2.3.2 Additional CMB datasets

Finally, we make decisions specific to the high multipole mode data of the South Pole Telescope (SPT) and Atacama Cosmology Telescope (ACT) collaborations. We consider purely adiabatic initial conditions, which provide predictions about secondary spectral contributions [20]. When the background data are taken to small enough scales the spectra from infrared source emission must be taken into account. The infrared (IR) spectra is dominated by Poisson power partially from source emission clustering at the smallest scales. Thus, a model for such effects must be subtracted out from the CMB power spectra. The resulting adaptations are representative of the considerations made during the process of checking the code for consistency with established results. It is also important to include a Big Bang nucleosynthesis (BBN) consistency check during the sampling in order to provide analysis consistent with helium abundance measurements, as proposed in Refs. [18, 56]. We remark that the ACT collaboration did not include the same BBN consistency condition used by SPT and our analysis. This explains why we find a slightly better constraint on N_{eff} than Ref. [13].

At this point, we include various models which vary the curvature Ω_k, effective neutrino number N_{eff}, and sum of the neutrino masses Σm_ν. This is done with a few simple modifications to CosmoMC (e.g. `params.ini`). Compare this with the dozens of changes in multiple files to account for the high-ℓ IR spectral contribution. Top hat priors are applied by setting minimum and maximum values on the allowed parameter space. There is also a best estimate applied with a stronger secondary range as the "top" of the "hat" (see Fig. 2.4). For the most part, the exact prior does not matter but we provide the ranges with the following notation (see Fig. 2.4):

$$(Estimate)^{+\sigma_{\text{Tight Upper}}}_{-\sigma_{\text{Tight Lower}}} \in [\text{Lower Bound}, \text{Upper Bound}]\,. \tag{2.23}$$

The prior for N_{eff} is $3.04^{+0.5}_{-0.5} \in [0,10]$ while the prior for Ω_k is $0^{+0.02}_{-0.02} \in [-0.2,0.2]$. Both easily provide enough freedom for a good fit in the parameter space. Finally, we also constrain the sum of the neutrino masses $\sum m_\nu$. To do this, we use a top hat prior on the fractional contribution of neutrinos to the total mass density, $f_\nu \equiv \Omega_\nu/\Omega_m$ of $0.05^{+0.01}_{-0.02} \in [0,0.5]$. Then we extract $\sum m_\nu$ from f_ν through the standard relation,

$$\sum m_\nu = 94\Omega_\nu h^2 \text{ eV} = 94h^2\Omega_m f_\nu \text{ eV}\,, \tag{2.24}$$

where $\Omega_\nu^2 \equiv \rho_\nu^0/\rho_{cr}$ is the neutrino contribution to the energy density [20]. Specifically, each value for f_ν in the MCMC chains must each be multiplied by $94h^2\Omega_m$ before the final Bayesian analysis is invoked (i.e. with `distparams.ini`).

Chapter 3

Results and Conclusions

3.1 Confirmation of correlation from cosmological data

We discuss the properties of the newfound parameter degeneracy, which is extracted from our analysis in Chapter 2. First of all, under the flat Universe scenario the constraint improves to $N_{eff} = 3.89 \pm 0.41$ at the 68% confidence level (see Table 2.1). This result suggests $N_{eff} = 3$ is inconsistent with the data with at least 95% confidence.

We then allow the curvature to vary to determine how assuming flatness affects the constraints on N_{eff}. Figure 3.1 demonstrates the correlation between Ω_k and N_{eff}, which agrees with the prediction from Section 2.1. Interestingly, the effect of the additional CMB datasets (ACT and SPT) increases the correlation between these parameters with respect to WMAP 7-year data alone. This may be due in part to the considerable improvement in N_{eff} whereas the uncertainty in the curvature of the Universe is not noticeably improved by the addition of small scale anisotropy measurements. These results suggest that an open universe with fewer neutrinos would look similar to a flat universe with more neutrinos. We also note that when including N_{eff} as a free parameter in the ΛCDM+Ω_k model, the 1σ constraint of $\Omega_k = -0.0023^{+0.0054}_{-0.0056}$ found in Ref. [11] does not

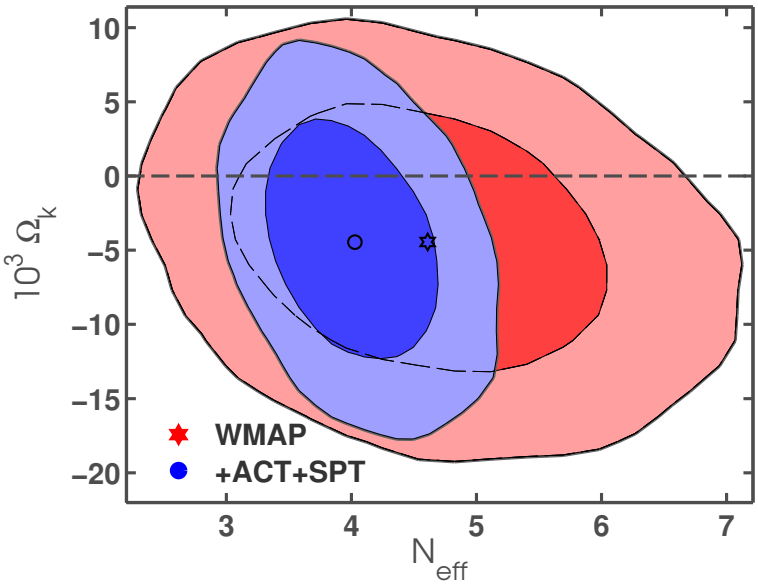

Figure 3.1 Correlation between Ω_k and N_{eff}. The credible intervals are given at the 68% and 95% confidence levels and the markers indicate the locations of the marginalized values. WMAP+BAO+H_0 is shown in red while WMAP+ACT+SPT+BAO+H_0 is in blue. Note that the effect of adding additional datasets is significant.

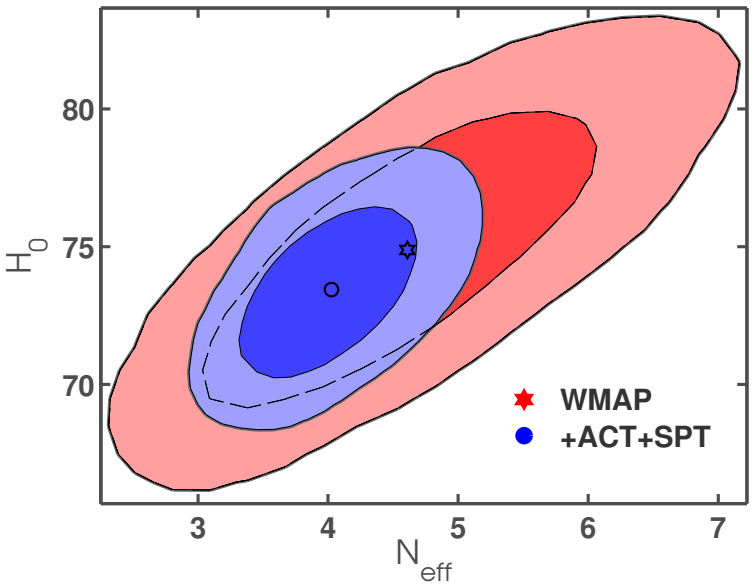

Figure 3.2 Correlation between H_0 and N_{eff}. The credible intervals are given at the 68% and 95% confidence levels and the markers indicate the locations of the marginalized values. WMAP+BAO+H_0 is shown in red while WMAP+ACT+SPT+BAO+H_0 is in blue. In this case the effect of adding additional datasets is also significant.

Parameter	WMAP7+N_{eff}+Ω_k	...+ACT+SPT
$100\Omega_b h^2$	2.26 ± 0.056	2.27 ± 0.045
$\Omega_c h^2$	0.136 ± 0.0169	0.129 ± 0.00915
Ω_Λ	0.721 ± 0.0179	0.723 ± 0.0158
n_s	0.9837 ± 0.0157	0.9863 ± 0.0147
τ	0.0887 ± 0.0148	0.0894 ± 0.0149
H_0(km/s/Mpc)	74.88 ± 3.40	73.44 ± 2.03
N_{eff}	4.61 ± 0.96	4.03 ± 0.45
$10^3\,\Omega_k$	-4.45 ± 5.85	-4.46 ± 5.24

Table 3.1 Summary of constraints while varying Ω_k and N_{eff}. All datasets include BAO and H_0 for improved parameter constraints. Errors are at the 68% CL. See Fig. 3.1.

deteriorate significantly for the same combination of datasets (i.e. WMAP+BAO+H_0). This is due to the presence of the BAO data and the H_0 prior in the analysis, since both probes are sensitive to the geometry of the Universe. Therefore, BAO and H_0 help to break the degeneracy between N_{eff} and Ω_k. The correlation is not as strong as we had expected. In fact, the correlation does not indicate a substantial problem with degeneracy. Furthermore the contour seems to favor a closed universe with $\Omega_k < 0$ rather than an open one. However, the correlation is still present and agreement with the prediction from Section 2.1.

Table 3.1 provides a summary of parameter values for runs where Ω_k and N_{eff} vary. Here we find $N_{eff} = 4.03 \pm 0.45$ and $10^3\Omega_k = -4.46 \pm 5.24$ at the 68% confidence level. Therefore, even when Ω_k is allowed to vary, $N_{eff} = 3$ is still disfavored with at least 95% confidence. Note that the increased value for H_0 is indicative of the known correlation between H_0 and Ω_k. We provide an equivalent marginalized contour plot of H_0 vs. N_{eff} to emphasize the connection (see Fig. 3.2).

Parameter	WMAP7+BAO+H_0	...+ACT+SPT
$100\Omega_b h^2$	2.26 ± 0.053	2.23 ± 0.038
$\Omega_c h^2$	0.112 ± 0.0036	0.111 ± 0.0029
Ω_Λ	0.719 ± 0.0182	0.726 ± 0.0154
n_s	0.968 ± 0.0124	0.963 ± 0.0092
τ	0.0897 ± 0.015	0.0873 ± 0.014
H_0(km/s/Mpc)	69.2 ± 1.6	69.9 ± 1.37
$\sum m_\nu$	< 0.57 eV	< 0.45 eV

Table 3.2 Summary of the constraint on the sum of the neutrino masses. All datasets include BAO and H_0 for improved parameter constraints. Errors are at the 68% CL except for $\sum m_\nu$, which is quoted as a 95% upper limit.

3.2 Neutrino mass

We now turn to the question of how well the datasets are able to constrain the sum of the neutrino masses $\sum m_\nu$. Table 3.2 shows the results from WMAP in the first column and the result of adding the additional datasets in the final column. Although the constraint greatly improves the two sigma limit for the masses, this is not enough to favor either the standard or inverted hierarchy (see Section 1.4). However, this is not a surprise because none of the datasets are sensitive enough on their own. Forthcoming data from the Planck experiment and other future experiments will likely improve the mass constraint [19].

Finally, we investigate the effect of assuming flatness while determining an upper bound on $\sum m_\nu$. We investigate two models. The first assumes three degenerate massive neutrinos, while the second allows for additional relativistic species accounted by $\Delta N_{eff} > 0$. We define the correlation coefficient ρ_{ij} as the ratio of the off-diagonal term of the covariance matrix σ_{ij} to the 1σ errors $\sigma_i \sigma_j$, so that for two parameters denoted by i and j we have $\rho_{ij} = \sigma_{ij}/\sigma_i \sigma_j$. Figure 3.3 shows that $\sum m_\nu$ and Ω_k are strongly correlated with a correlation coefficient of $\rho_{\Omega_k \sum m_\nu} = 0.78$ for both models ($\Delta N_{eff} = 0$ and $\Delta N_{eff} > 0$). Furthermore, the degeneracy considerably increases the uncertainty in the sum of the neutrino masses. In fact, with $\Omega_k \neq 0$ the 95% upper limit on $\sum m_\nu$ more

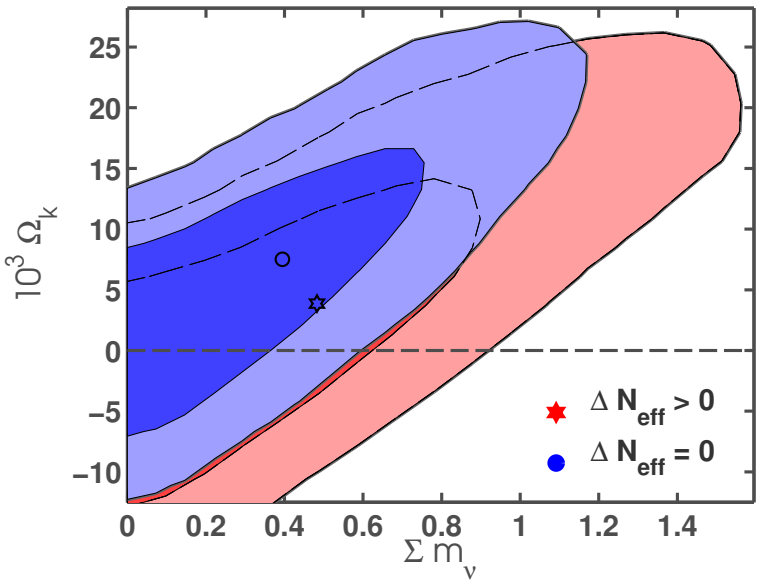

Figure 3.3 Comparison of the correlation between Ω_k and $\sum m_\nu$ under the two ΔN_{eff} models under consideration. The model with three massive neutrinos is shown in blue while the model with additional relativistic species is in red. Intervals are given at the 68% and 95% confidence levels and markers indicate the locations of the marginalized values. Datasets include WMAP7+ACT+SPT+BAO+H_0. The addition of curvature allows $\sum m_\nu$ to be more than twice the previous constraint with $\Omega_k = 0$.

than doubles with respect to the flat case: with $\sum m_\nu < 0.95$ eV for the model assuming only three massive neutrinos and $\sum m_\nu < 1.19$ eV for $\Delta N_{eff} > 0$. The strong correlation between curvature and mass is expected because massive neutrinos are still relativistic at decoupling so they act as additional radiation (c.f. Ref. [48]). As a consequence the presence of massive neutrinos shifts both the time of matter-radiation equality a_{eq} and the position of CMB peaks. This effect can be compensated for by a change in the geometry of the Universe, which weakens the constraints on both $\sum m_\nu$ and Ω_k. See Table 3.3 for a summary of cosmological parameters when curvature and massive neutrinos are considered.

The constraint on the sum of the neutrino masses with the combined datasets is is an important result by itself (see Section 1.4). However, the effect of curvature on the neutrino mass is insightful, especially when compared with the $\Delta N_{eff} > 0$ model. Both models produce roughly the same

Parameter	$\Delta N_{eff} = 0$	$\Delta N_{eff} > 0$
$100\Omega_b h^2$	2.24 ± 0.043	2.26 ± 0.049
$\Omega_c h^2$	0.118 ± 0.0063	0.134 ± 0.0105
Ω_Λ	0.711 ± 0.0216	0.703 ± 0.0239
n_s	0.967 ± 0.011	0.982 ± 0.015
τ	0.0864 ± 0.0144	0.0890 ± 0.0145
H_0(km/s/Mpc)	70.6 ± 1.62	73.1 ± 2.03
$10^3\,\Omega_k$	7.52 ± 7.74	3.46 ± 8.69
$\sum m_\nu$	< 0.95 eV	< 1.19 eV
ΔN_{eff}	0	0.995 ± 0.430

Table 3.3 Summary of the constraint on the sum of the neutrino masses when $\Omega_k \neq 0$. ΔN_{eff} is an additional relativistic contribution after considering 3.046 massive neutrinos. Datasets include WMAP7+ACT+SPT+BAO+H_0. Errors are at the 68% CL except for $\sum m_\nu$, which is quoted as a 95% upper limit.

correlation effect but the one with additional relativistic neutrinos has a "pull" toward $\Omega_k < 0$. This is significant because the correlations are opposing each other so that the mass favors an open universe and the effective neutrino number favors a closed universe. However, it should be noted that N_{eff} and ΔN_{eff} are not the same parameter! Indeed, a model with all relativistic neutrinos and a model with massive neutrinos are intrinsically different. This means we cannot make a plot of Ω_k vs. ΔN_{eff} similar to Fig. 3.1. The parameter still has a noticeable effect on other cosmological parameters, such as Ω_k and $\sum m_\nu$, but may not have any correlation between them.

3.3 Implications of assuming flatness

The resolution of the high effective neutrino number in cosmology remains an open question. However, additional neutrinos may be due to parameter degeneracy or other issues in statistical analysis rather than new physics. In this thesis we have discussed some of the interesting physics behind neutrino cosmology and contributed to the rich subject. The focus has been an argument for correlation between the number of effective neutrinos N_{eff} and the curvature of the Universe

Ω_k, which arises from the effect of these parameters on distance measurements. The qualitative argument is confirmed by a statistical analysis of CMB anisotropy measurements using CosmoMC.

Indeed, we have shown that there is a correlation between N_{eff} and Ω_k that gets stronger when SPT and ACT datasets are added to WMAP alone. However, even when Ω_k is allowed to vary, $N_{eff} = 3$ is still disfavored by the data with 95% confidence. Although the correlation favors a closed universe with $\Omega_k < 0$, if CMB data were to favor open models then the neutrino number would decrease as predicted. Perhaps the same element of the data that favors a closed universe may also be responsible for the trend toward a higher N_{eff}. More importantly, we discovered strong correlation between curvature and the sum of the neutrino masses.

Future experiments will provide further insight into both N_{eff} and $\sum m_\nu$ [57]. Our results are consistent with the current understanding of the data available. The strongest constraints on these parameters from the statistical analysis assuming a flat universe are $N_{eff} = 3.89 \pm 0.41$ and $\sum m_\nu < 0.45$ eV with 95% confidence level using WMAP7+ACT+SPT+BAO+H_0. The constraints are weakened by degeneracy with the curvature parameter Ω_k. However, this still represents the continued effort toward significant improvements on parameter constraints in cosmology. Although the sum of the neutrino masses is significantly improved from the WMAP 7-year result of $\sum m_\nu < 0.57$ eV, the constraint is far from being sensitive enough to rule out one of the mass hierarchies. Furthermore, we have shown that the mass uncertainty more than doubles when $\Omega_k \neq 0$. Based on our results and the estimated quality of data for Planck and other experiments, it should be possible to determine the existence or nonexistence of sterile radiation to greater confidence in the near future.

3.4 Future work

There are many directions for similar research involving parameter constraints under different models, but the scope of this work is fairly self-contained so we have chosen to move on to other problems. The correlation measures should be put into proper perspective. They are statistical tools used to explore various cosmological models. In other words correlation is just a correlation and does not "favor" anything. In this respect the greatest improvements on cosmological models will take place as future experiments are able to decrease parameter uncertainty by orders of magnitude. New and innovative designs must be sought out by collaborations hoping to achieve such results. This is a rich area of research that will continue to influence other areas of physics, as has been seen by the insights emphasized in Chapter 1, especially relating to the neutrino mass hierarchy.

For students interested in this avenue of theoretical and computational cosmology we suggest a collaborative environment. It is much more effective to facilitate this kind of research under a group with experience with cluster computing. In the age of information the learning process is simply a matter of choice, which may be pursued through the references provided. An example of a similar project would be to investigate the effects of baryon acoustic oscillations (BAO) and gravitational lensing in possibly breaking the degeneracy between neutrino parameters. We suspect these topics will have advanced significantly in ten years. Hopefully, by that time the source of effective neutrinos will no longer be an open question in cosmology.

We conclude this thesis by briefly describing our current research focus. We have become interested in the cosmic geometry and topology of the Universe. Currently, statistical models only consider the possibility of the flat ($\Omega_k = 0$), spherical ($\Omega_k < 0$), and hyperbolic ($\Omega_k > 0$) geometries. However, under the geometrization conjecture and the work of Thurston and others there are five additional unique geometries for spatial 3-Manifolds [58]. We do not provide details here but most of the work in this area has been mathematical in nature with only a few applications in cosmology. Perhaps there is good reason for this because the cosmological principle, which

assumes spatial isotropy and homogeneity (i.e. to a good approximation the Universe looks the same same in every direction from any reference point). Nonetheless, in this theoretical project we hope to constrain generalized curvature parameters in these FRW-like spacetimes in order to provide an additional check on the validity of assuming flatness in general.

Bibliography

[1] A. Smith *et al.*, "The Impact of Assuming Flatness in the Determination of Neutrino Properties from Cosmological Data," Phys.Rev. **D85,** 123521 (2012).

[2] Z. Hou, R. Keisler, L. Knox, M. Millea, and C. Reichardt, "How Additional Massless Neutrinos Affect the Cosmic Microwave Background Damping Tail," arXiv:1104.2333 (2011).

[3] M. Archidiacono, E. Calabrese, and A. Melchiorri, "The Case for Dark Radiation," Phys.Rev. **D84,** 123008 (2011).

[4] E. Giusarma, M. Archidiacono, R. de Putter, A. Melchiorri, and O. Mena, "Constraints on massive sterile plus active neutrino species in non minimal cosmologies," arXiv:1112.4661 (2011).

[5] R. R. Volkas, "Introduction to sterile neutrinos," Prog.Part.Nucl.Phys. **48,** 161–174 (2002).

[6] M. Shaposhnikov, "Dark Matter: The Case of Sterile Neutrino," astro-ph/0703673 (2007).

[7] R. Sanders, "Neutrinos as cluster dark matter," Mon.Not.Roy.Astron.Soc. **380,** 331–338 (2007).

[8] J. Hamann, S. Hannestad, G. G. Raffelt, I. Tamborra, and Y. Y. Wong, "Cosmology seeking friendship with sterile neutrinos," Phys.Rev.Lett. **105,** 181301 (2010).

[9] C. Giunti and M. Laveder, "3+1 and 3+2 Sterile Neutrino Fits," Phys.Rev. **D84,** 073008 (2011).

[10] W. Hu and S. Dodelson, "Cosmic microwave background anisotropies," Ann.Rev.Astron.Astrophys. **40,** 171–216 (2002).

[11] E. Komatsu *et al.*, "Seven-Year Wilkinson Microwave Anisotropy Probe (WMAP) Observations: Cosmological Interpretation," Astrophys.J.Suppl. **192,** 18 (2011).

[12] R. Keisler *et al.*, "A Measurement of the Damping Tail of the Cosmic Microwave Background Power Spectrum with the South Pole Telescope," Astrophys.J. **743,** 28 (2011).

[13] J. Dunkley *et al.*, "The Atacama Cosmology Telescope: Cosmological Parameters from the 2008 Power Spectra," Astrophys.J. **739,** 52 (2011).

[14] S. Joudaki, "Constraints on Neutrino Mass and Light Degrees of Freedom in Extended Cosmological Parameter Spaces," arXiv:1202.0005 (2012).

[15] C. Howlett, A. Lewis, A. Hall, and A. Challinor, "CMB power spectrum parameter degeneracies in the era of precision cosmology," JCAP **1204,** 027 (2012).

[16] D. Spergel *et al.*, "First year Wilkinson Microwave Anisotropy Probe (WMAP) observations: Determination of cosmological parameters," Astrophys.J.Suppl. **148,** 175–194 (2003).

[17] E. Alizadeh and C. M. Hirata, "How to detect gravitational waves through the cross-correlation of the galaxy distribution with the CMB polarization," arXiv:1201.5374 (2012).

[18] J. Hamann, J. Lesgourgues, and G. Mangano, "Using BBN in cosmological parameter extraction from CMB: A Forecast for PLANCK," JCAP **0803,** 004 (2008).

[19] P. Ade *et al.*, "Planck Early Results: The Planck mission," arXiv:1101.2022 (2011).

[20] S. Dodelson, *Modern cosmology* (Amsterdam, Netherlands: Academic Pr., 2003).

[21] D. Baumann, "TASI Lectures on Inflation," arXiv:0907.5424 (2009).

[22] NASA / COBE Science Team, "CMB Blackbody Spectrum," http://lambda.gsfc.nasa.gov/product/cobe/firas_image.cfm (2009).

[23] C. Reichardt *et al.*, "Constraints on the High-l Power Spectrum of Millimeter-wave Anisotropies from APEX-SZ," Astrophys.J. **701,** 1958–1964 (2009).

[24] J. Fowler *et al.*, "The Atacama Cosmology Telescope: A Measurement of the 600 < ell < 8000 Cosmic Microwave Background Power Spectrum at 148 GHz," Astrophys.J. **722,** 1148–1161 (2010).

[25] X. Dupac, "Cosmology from Cosmic Microwave Background fluctuations with Planck," astro-ph/0701523 (2007).

[26] NASA / WMAP Science Team, "Timeline of the Universe," http://map.gsfc.nasa.gov/media/060915/index.html (2011).

[27] J. Hartle, *Gravity: An introduction to Einstein's general relativity* (Addison-Wesley, Boston, 2003).

[28] S. Hannestad, "Introduction to neutrino cosmology," Prog.Part.Nucl.Phys. **57,** 309–323 (2006).

[29] E. Calabrese, D. Huterer, E. V. Linder, A. Melchiorri, and L. Pagano, "Limits on Dark Radiation, Early Dark Energy, and Relativistic Degrees of Freedom," Phys.Rev. **D83,** 123504 (2011).

[30] Y. Fukuda *et al.*, "Measurements of the solar neutrino flux from Super-Kamiokande's first 300 days," Phys.Rev.Lett. **81,** 1158–1162 (1998).

[31] K. Kodama *et al.*, "Observation of tau neutrino interactions," Phys.Lett. **B504,** 218–224 (2001).

[32] S. Agarwal and H. A. Feldman, "The Effect of Massive Neutrinos on Matter Power Spectrum," arXiv:1006.0689 (2010).

[33] F. De Bernardis, T. D. Kitching, A. Heavens, and A. Melchiorri, "Determining the Neutrino Mass Hierarchy with Cosmology," Phys.Rev. **D80,** 123509 (2009).

[34] R. Jimenez, T. Kitching, C. Pena-Garay, and L. Verde, "Can we measure the neutrino mass hierarchy in the sky?," JCAP **1005,** 035 (2010).

[35] S. Hannestad, "Neutrino masses and the number of neutrino species from WMAP and 2dFGRS," JCAP **0305,** 004 (2003).

[36] S. Hannestad, A. Mirizzi, G. G. Raffelt, and Y. Y. Wong, "Neutrino and axion hot dark matter bounds after WMAP-7," JCAP **1008,** 001 (2010).

[37] M. Cirelli and A. Strumia, "Cosmology of neutrinos and extra light particles after WMAP3," JCAP **0612,** 013 (2006).

[38] C. Zunckel and P. Ferreira, "Conservative Estimates of the Mass of the Neutrino from Cosmology," JCAP **0708,** 004 (2007).

[39] U. Seljak, A. Slosar, and P. McDonald, "Cosmological parameters from combining the Lyman-alpha forest with CMB, galaxy clustering and SN constraints," JCAP **0610,** 014 (2006).

[40] M. A. Acero and J. Lesgourgues, "Cosmological constraints on a light non-thermal sterile neutrino," Phys.Rev. **D79,** 045026 (2009).

[41] F. De Bernardis, P. Serra, A. Cooray, and A. Melchiorri, "An improved limit on the neutrino mass with CMB and redshift-dependent halo bias-mass relations from SDSS, DEEP2, and Lyman-Break Galaxies," Phys.Rev. **D78,** 083535 (2008).

[42] I. Tereno *et al.*, "CFHTLS weak-lensing constraints on the neutrino masses," Astron.Astrophys. **500,** 657–665 (2009).

[43] Y. Gong, T.-J. Zhang, T. Lan, and X.-L. Chen, "Dark energy and neutrino mass constraints from weak lensing, supernova, and relative galaxy ages," arXiv:0810.3572 (2008).

[44] B. A. Reid, L. Verde, R. Jimenez, and O. Mena, "Robust Neutrino Constraints by Combining Low Redshift Observations with the CMB," JCAP **1001,** 003 (2010).

[45] M. Shimon, S. Sadeh, and Y. Rephaeli, "Neutrino Mass Inference from SZ Surveys," arXiv:1009.4110 (2010).

[46] R. Sachs and A. Wolfe, "Perturbations of a cosmological model and angular variations of the microwave background," Astrophys.J. **147,** 73–90 (1967).

[47] D. W. Hogg, "Distance measures in cosmology," astro-ph/9905116 (1999).

[48] J. Lesgourgues and S. Pastor, "Massive neutrinos and cosmology," Phys.Rept. **429,** 307–379 (2006).

[49] L. Verde, "Statistical methods in cosmology," Lect.Notes Phys. **800,** 147–177 (2010).

[50] A. X. Gonzalez-Morales, R. Poltis, B. D. Sherwin, and L. Verde, "Are priors responsible for cosmology favoring additional neutrino species?," arXiv:1106.5052 (2011).

[51] NASA / WMAP Science Team, "Internal Linear Combination Map and WMAP Seven-Year TT Power Spectra," http://lambda.gsfc.nasa.gov/product/map/current/m_images.cfm (2010).

[52] A. Lewis and S. Bridle, "Cosmological parameters from CMB and other data: A Monte Carlo approach," Phys.Rev. **D66,** 103511 (2002).

[53] A. Lewis, A. Challinor, and A. Lasenby, "Efficient computation of CMB anisotropies in closed FRW models," Astrophys.J. **538,** 473–476 (2000).

[54] W. J. Percival *et al.*, "Baryon Acoustic Oscillations in the Sloan Digital Sky Survey Data Release 7 Galaxy Sample," Mon.Not.Roy.Astron.Soc. **401,** 2148–2168 (2010), 21 pages, 15 figures, submitted to MNRAS.

[55] A. G. Riess *et al.*, "A 3% Solution: Determination of the Hubble Constant with the Hubble Space Telescope and Wide Field Camera 3," Astrophys.J. **730,** 119 (2011).

[56] K. Ichikawa and T. Takahashi, "Revisiting the constraint on the helium abundance from cmb," Phys.Rev. **D73,** 063528 (2006).

[57] C. Carbone, L. Verde, Y. Wang, and A. Cimatti, "Neutrino constraints from future nearly all-sky spectroscopic galaxy surveys," JCAP **1103,** 030 (2011).

[58] P. Scott, "The geometries of 3-manifolds," Bull. London Math. Soc. **15,** 401–487 (1983).

Index